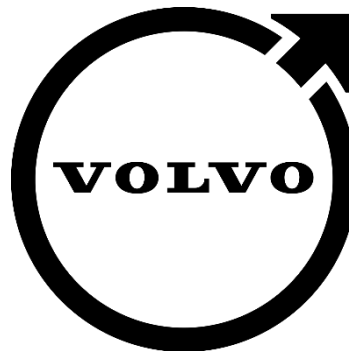




Master's Degree in Engineering for Mobility and Safety
(M2S)

Master Thesis



Modelling of gear surface roughness impact on electrified
transmissions' efficiency

Ignacio Victoria Rodríguez

Supervisor:
Foteini Xanthi

Madrid
August 2022

Declaro, bajo mi responsabilidad, que el Proyecto presentado con el título
“Modelling of gear surface roughness impact on electrified transmissions’
efficiency” en la ETS de Ingeniería - ICAI de la Universidad Pontificia Comillas
en el

curso académico 2021/22 es de mi autoría, original e inédito y
no ha sido presentado con anterioridad a otros efectos. El Proyecto no es
plagio de otro, ni total ni parcialmente y la información que ha sido tomada
de otros documentos está debidamente referenciada.



Fdo.: Ignacio Victoria Rodríguez

Fecha: 22/08/2022

Autorizada la entrega del proyecto

EL DIRECTOR DEL PROYECTO



[Foteini Xanthi \(Aug 22, 2022 07:57 GMT+2\)](#)

Fdo.: Foteini Xanthi

Fecha: 22/08/2022

Results in Engineering

Modelling of gear surface roughness impact on gear meshing efficiency

--Manuscript Draft--

Manuscript Number:	RINENG-D-22-00891
Full Title:	Modelling of gear surface roughness impact on gear meshing efficiency
Short Title:	
Article Type:	Full Length Article
Section/Category:	Mechanical
Keywords:	efficiency; gears; surface deformation; lubrication; Contact Mechanics
Corresponding Author:	Ignacio Victoria Rodriguez, M.Eng & M.Sc. Volvo Car Corporation Göteborg, Västra Götaland SWEDEN
Corresponding Author Secondary Information:	
Corresponding Author's Institution:	Volvo Car Corporation
Corresponding Author's Secondary Institution:	
First Author:	Ignacio Victoria Rodriguez, M.Eng & M.Sc.
First Author Secondary Information:	
Order of Authors:	Ignacio Victoria Rodriguez, M.Eng & M.Sc. Foteini Xanthi, M.Eng & M.Sc.
Order of Authors Secondary Information:	
Abstract:	<p>This publication models gear meshing efficiency with a novel approach combining several propositions from different fields into a single conglomerate. The model calculates lubrication regime, pressure distribution with complete and partial surface separation, surface contact stress; sub-surface stress; bilateral surface deformation and losses incurred during 2D gear rough deformable line contact within very limited computational time. The pressure variation in the lubricant is derived from a 2D static approximation of the Navier-Stokes solution which disregards the transit of fluid through the z-coordinate for a cylindrical reference, aligning the radial and azimuthal axis with the equivalent circumference of the contact. The lubrication regime is a modified proposition of a relatively new estimation method and the contact stress and surface deformation have been adapted to accept any type of surface from the original curved-against-flat surface set-up. The losses are then broken down into plastic surface deformation, sliding friction and rolling resistance losses. The novelty lies on the speed at which the model operates with numerical and algebraic solvers whilst combining these different characteristics with a high precision, reaching similar conclusions to full 3D dynamic simulations whilst also combining several aspects of contacts which would typically be found in separate models and publications.</p>
Suggested Reviewers:	<p>Isaac Hong, Mechanical Engineering Research Scientist, The Ohio State University hong.250@osu.edu Referenced as a possible reviewer by an external independent expert.</p> <p>Michael Handschuh, Mechanical Engineering Research Scientist, The Ohio State University handschuh.1@osu.edu Proposed by an external, independent expert</p> <p>Praviz Merati, Mechanical Engineering Professor, Western Michigan University praviz.merati@wmich.edu Cited author in the manuscript</p>

Additional Information:	
Question	Response
<p>Results in Engineering is an open access journal which charges an Article Publishing Charge (APC) to cover the cost associated with the publication process.</p> <p>All articles published Open Access will be immediately and permanently free on ScienceDirect for users to read, download, and use in accordance with the author's selected Creative Commons user license.</p> <p>As an Author, I acknowledge I need to pay the Article Publishing Charge if my manuscript is accepted for publication.</p>	Yes

Volvo Car Corporation
405 31
Göteborg, Sweden

Dr. Antonio García Martínez
Polytechnic University of Valencia.
Valencia, Spain

Prof. Suresh C. Pillai,
Atlantic Technological
University – Sligo
Sligo, Ireland

Dr. Norman Toy
Engineering &
Scientific Innovations
Inc, Fairfield, Ohio,
USA

July 26th, 2022

Dear Professor, Doctors and Editors,

We wish to submit an original research article entitled “*Modelling of gear surface roughness impact on gear meshing efficiency*” for consideration by Results in Engineering.

We confirm that this work, which contains part of Ignacio Victoria Rodríguez’s unpublished Master Thesis, is original and has not been published elsewhere, nor is it currently under consideration for publication elsewhere.

This here paper consolidates several different aspects of gear contacts into one singular, holistic model which we believe will be appealing to the readers of Results in Engineering. From our literature research we have found no paper linking surface roughness with gear mesh efficiency. This novel approach relies on modelling and applied computer methods to estimate consistently and reliably the lubrication regime, contact mechanics, pressure across the oil film and efficiency, in a holistic way which we have not seen replicated across the literature.

We have no conflicts of interest to disclose.

Sincerely,

Ignacio Victoria Rodríguez

ignacio.victoria.rodrique@volvocars.com

Master Thesis Student,
Volvo Car Corporation

Foteini Xanthi

foteini.xanthi@volvocars.com

Advanced Engineering Lead in Torque Transfer,
Volvo Car Corporation

Author Agreement Statement

We the undersigned declare that this manuscript is original, has not been published before and is not currently being considered for publication elsewhere.

We confirm that the manuscript has been read and approved by all named authors and that there are no other persons who satisfied the criteria for authorship but are not listed. We further confirm that the order of authors listed in the manuscript has been approved by all of us.

We understand that the Corresponding Author is the sole contact for the Editorial process. He/she is responsible for communicating with the other authors about progress, submissions of revisions and final approval of proofs Signed by all authors as follows:

Ignacio Victoria Rodríguez

ignacio.victoria.rodrique@volvocars.com

Master Thesis Student,
Volvo Car Corporation

Corresponding Author,

Foteini Xanthi

foteini.xanthi@volvocars.com

Advanced Engineering Lead in Torque Transfer,
Volvo Car Corporation

Declaration of interests

The authors declare that they have no known competing financial interests or personal relationships that could have appeared to influence the work reported in this paper.

The authors declare the following financial interests/personal relationships which may be considered as potential competing interests:

Ignacio Victoria Rodriguez reports financial support was provided by Volvo Car Corporation. Foteini Xanthi reports financial support was provided by Volvo Car Corporation. Foteini Xanthi reports a relationship with Volvo Car Corporation that includes: employment. Ignacio Victoria Rodriguez reports a relationship with Volvo Car Corporation that includes: funding grants. No existing conflicts of interest

Highlights

- The highlights of this paper are:
- Gear meshing efficiency with a novel approach
- The lubrication regime is a modified proposition
- Surface deformation adapted to accept any type of surface
- Numerical and algebraic solvers
- Losses incurred during 2D gear rough deformable line contact

[Click here to view linked References](#)

Title

Modelling of gear surface roughness impact on gear meshing efficiency

Authors

Ignacio Victoria Rodríguez, Foteini Xanthi

ignacio.victoria.rodriguez@volvocars.com Volvo Cars, 405 31 Göteborg, Sweden

foteini.xanthi@volvocars.com Volvo Cars, 405 31 Göteborg, Sweden

Keywords

Efficiency, gears, surface deformation, lubrication, contact mechanics

Abstract

This publication models gear meshing efficiency with a novel approach combining several propositions from different fields into a single conglomerate. The model calculates lubrication regime, pressure distribution with complete and partial surface separation, surface contact stress; sub-surface stress; bilateral surface deformation and losses incurred during 2D gear rough deformable line contact within very limited computational time. The pressure variation in the lubricant is derived from a 2D static approximation of the Navier-Stokes solution which disregards the transit of fluid through the z-coordinate for a cylindrical reference, aligning the radial and azimuthal axis with the equivalent circumference of the contact. The lubrication regime is a modified proposition of a relatively new estimation method and the contact stress and surface deformation have been adapted to accept any type of surface from the original curved-against-flat surface set-up. The losses are then broken down into plastic surface deformation, sliding friction and rolling resistance losses. The novelty lies on the speed at which the model operates with numerical and algebraic solvers whilst combining these different characteristics with a high precision, reaching similar conclusions to full 3D dynamic simulations whilst also combining several aspects of contacts which would typically be found in separate models and publications.

1. Introduction

Although a pair of gear meshing is one of the most efficient means of mechanical power transfer, it's paramount the underlying mechanism found therein are fully understood and in turn modified to suit today's needs. As of today, gear efficiency is mainly studied through simulation software, which, at the expense of great computational power can yield remarkable results.

Despite this awing capacity, surface roughness is rarely studied with simulation tools, since the element size required increases the computational cost tremendously, alas, it is normally modelled for each specific mechanism under study, most commonly surface deformation or temperature. As such, very rarely do we see a model which encompasses most mechanisms which act upon a surface such as the one presented in this publication, focusing mainly on the effect of lubrication, deformation and roughness on efficiency on both a macro and microscopic level.

To tackle this complex problem from multiple points of view firstly, a literature review of across the different model fields was performed in section 2, studying separately dry contact deformable models (section 2.1), the challenge of estimating and accurate friction coefficient and modelling the rolling and sliding forces (section 0); The accuracy and reliability of lubrication regime approximations is reviewed in section 2.3

whilst the relevance of the pressure across the lubricant and its complex solutions are discussed in section 2.4. These proposed models and formulas were adapted to this particular case, as seen in section 3. Which was in turn followed by a model-by-module and global evaluation presented in section 4. Finally, the modular nature of the model allows for customization and both modular and system optimization, tailoring the model for very specific needs easily from a flexible based, presented in this publication.

2. Theoretical background

In this section a summary of the publications referenced is provided along with some comments and their influence in the final model. Firstly, a rough bilaterally deformable contact was modelled and is presented in section 2.1. This was in turn followed up with a research effort into rolling and sliding effects, to complement the contact stress with off-plane shear components and the results are shown in section 0. Lubrication and its effects were first introduced later after a review of the existing literature and are presented in section 2.3. Once the lubrication regime was accurately established the effect of pressure on the oil film and the surface was studied, as shown in section 2.4, completing the entourage of physical elements directly acting on the surfaces.

2.1. Dry rough contact model numerical approximation

In the references [1] and [2], the surface deformation eq.(1 resulting from two rough surfaces was approximated with an elliptical-to-half-space contact, considering both to be deformable solid with a formulation derived from [3].

Expanding this formulation to an elliptical-to-half-space contact, considering both to be deformable solid with a formulation derived from [3]. In it, the compliance matrix eq.(2 relies in a formulation based in the half-cell size of the surface profile and the logarithmic stiffness formulation. This simplifies the local contact stress formulation to a matrix operation, as presented in eq.(3. Consequently, the contact force can be computed as in eq.(4 which allows for a numerical solver implementation by lowering each surface into each other.

Furthermore, the author [1] describes a set of equations to calculate sub-surface shear stress based on Johnson's equations [4] which yields a polynomial formulation [1] as shown in eq.. Thus, reducing computational cost and having a maximum at $z=a$, where the shear stress will be 20.7% of the surface stress, alas, the shear stress contour line will mimic the surface. A minor modification allows for the computation of elastic and plastic deformation eq.(6, considering the Von-Misses' stress principle.

This section can be summarized into a general dry-rough surface contact model which relies on a matrix equation for the contact stress which allows for a quick and efficient numerical solver base.

$$\bar{u}_{zi} = \frac{1}{\pi E^*} \sum_{j=1}^n C_{ij} p_j \quad (1)$$

Where \bar{u}_{zi} stands for the deformation of surface i , and is calculated by the E^* Reduced Young's Modulus and the sum of C_{ij} , the compliance matrix of surface i and j and p_j contact stress in surface j . For C_{ij} the following equation is used:

$$C_{ij} = (x_{\Delta} - a_L) \left[\ln \left(\frac{x_{\Delta} - a_L}{a_L} \right) \right]^2 - (x_{\Delta} + a_L) \left[\ln \left(\frac{x_{\Delta} + a_L}{a_L} \right) \right]^2 + C_o |x_{\Delta} - x_j| \quad (2)$$

Where x_{Δ} is the absolute value of the difference of coordinates along the x-axis and a_L is half-cell size. Following, the stress vector across the surface contact \bar{p} is calculated:

$$\bar{p} = \pi E^* C^{-1} (\delta - \bar{h}) \quad (3)$$

where δ is the approach distance and \bar{h} the height difference between both surfaces. Continuing, the contact force F_C will be:

$$F_C = \int \bar{p} dx \quad (4)$$

To calculate the sub-surface stress τ_i at each point:

$$\tau_i = -\frac{p_i}{a} (z_{surf} - z_{surf}^2 (a^2 + z_{surf}^2)^{-\frac{1}{2}}) \quad (5)$$

Where p_i is the contact stress in point i , z_{surf} stands for the depth from the surface and a is the differential size. Finally, translating all stress to the same plane, the plastic stress σ_p :

$$\sigma_p = \sigma_{VM} - \sigma_e \quad (6)$$

Where σ_{VM} is the equivalent Von Misses stress and σ_e the elastic stress.

2.2. Rolling and sliding forces

In the reference [5], the friction coefficient of the lubricant is described with a 94% accuracy and a model error for the acting forces below 0.1%. The friction coefficient approximation eq.(7) relies in commonly accepted parameters and a custom-made vector $b_i \mid i = [1,2, \dots 9]$ belong to a 9-element coefficient vector derived from a linear regression of the lubricant properties, which in the reference [5] is described as the standard FZG set-up lubricant.

This section encompasses an ultra-precise formulation of the friction coefficient based on the lubricant.

$$\begin{cases} \mu = e^{f(SR, P_h, \nu_o, S)} P_h^{b_2} |SR|^{b_3} V_e^{b_6} \nu_o^{b_7} R^{b_8} \\ f(SR, P_h, \nu_o, S) = b_1 + b_4 |SR| P_h \log_{10}(\nu_o) + b_5 e^{-|SR| P_h \log_{10}(\nu_o)} + b_9 e^S \end{cases} \quad (7)$$

Such that μ is the friction coefficient; SR is the slip-to-rolling ratio upon the teeth meshing, P_h is the maximum Hertzian contact pressure; ν_o is the absolute viscosity (in cPs for this application) at the oil inlet temperature; V_e is the entraining velocity; R is the equivalent radius of the; S is the equivalent RMS surface roughness. The equivalent RMS of both surfaces can be computed as:

$$S = RMS_{total} = \sqrt{\sum_{i=1}^n (RMS_i)^2} \quad (8)$$

Where S is the overall root mean square surface roughness and RMS_i is the root mean square surface roughness of each surface (either 1 or 2).

Since the reference [5] considers a deformable-ball or a rigid and perfectly flat disc contact, the formulation was modified to consider a bilateral deformable contact of any geometry as seen in eq. **Error! Reference source not found.**, assuming both surfaces are a combination of different waveforms which can be represented as a Fast Fourier Transform.

In the same reference as the friction coefficient [5] a global definition for the sliding and rolling forces in a contact are perpendicular to the pressure line. This implementation of the friction coefficient agrees with the approximations made in [6] where it was shown μ is correlated with the slide-to-roll ratio.

Other papers [7] estimate a loss coefficient purely dependant on the friction the gears teeth experiment as one moves over the other, in other words, friction as a function of the contact band position along the flank. Said approximation is valid for global approaches, however, when it comes to the study of surfaces and their contacts it's a vast simplification. Similarly, the friction coefficient was sometimes estimated based

on classical EHL parameters as explained in [8], which, although is fairly accurate for ball-to-disc contacts it presents problems in more complex set-ups where the contact area isn't as clear. The rolling force is derived in [5] from an empirical formula from [9] and it's presented in eq. **Error! Reference source not found.** The lubricant properties are highly dependent on the thermal factor depicted in eq. **Error! Reference source not found.**, however, the definition is given in a different publication from the same author [10] and is shown in eq. **Error! Reference source not found.** Since no thermal events on the lubricant were considered, it was assumed the derivative would be null and therefore the coefficient tends to 1.

Having, thus, characterized the macro-level properties of the lubricant, a Navier-Stokes approximate solution may characterize the pressure field of the lubricant when both teeth have meshed. The rolling force goes as follows:

$$F_r = \frac{4.318\varphi_T(\tilde{G}\tilde{U})^{0.658}\tilde{Q}^{0.0126}R}{\alpha_{PV}} \quad (9)$$

$$1 - 13.2\frac{P_h}{E^*}(L^*)^{0.42} \quad (10)$$

$$\varphi_T = \frac{1}{1 + 0.213(1 + 2.23SR^{0.83})(L^*)^{0.64}} \quad | \quad L^* = -\frac{\partial v}{\partial T_o} \frac{(V_e)^2}{K_f}$$

Such that F_r is the rolling resistance; φ_T is the thermal reduction factor to account for the effect of temperature rise at high-speed conditions [5], however, said value isn't disclosed in the reference, but it is described at length in [10]. \tilde{G} is the dimensionless material parameter; \tilde{U} is the dimensionless speed parameter; \tilde{Q} is the dimensionless load parameter and α is the pressure viscosity coefficient

2.3. Lubrication regime

Traditionally, lubrication parameters were used to estimate the separation between surfaces. In turn, the parameter h_o can be estimated from traditional EHL theory if h_o was considered to be the fluid film present between two lubricated surfaces. Said parameter, traditionally labelled Δh , relies on the deformation of surface peaks due to pressurization of the fluid as it's being entrained, causing a Venturi between both surfaces [11]. Said height, would traditionally be used to calculate the parameter Λ , which could partly predict the type of contact between both surfaces.

That prediction was improved upon in [12], to the defining parameter Λ^* , said parameter could predict a EHL contribution of 60-80% in mixed lubrication conditions for any ball-on-disc contact and correctly predict a 100% EHL contact when full-film lubrication was tested. Furthermore, said parameter, Λ^* , accounted for the roughness of real engineering surfaces, although not bilaterally, one surface was considered to be perfectly flat and infinitely rigid [12]. In said publication [12] and PhD Thesis [13], the authors go into a lot of detail explaining this new parameter Λ^* , which can be considered as the ratio between the total surface deformation and the peak surface roughness, with the formulation presented in eq.(11).

$$\Lambda^* = \frac{h^*}{S_{pk}} \quad (11)$$

Where Λ^* is the aforementioned lubrication regime estimator where $\Lambda^* \geq 1$ implies full EHL lubrication whilst $\Lambda^* < 1$ implies boundary lubrication or mixed lubrication. The total surface separation is represented by h^* and the peak surface roughness is represented by S_{pk} in the equation. Where h_m is the minimal surface separation plus the deformed asperity height variation as seen in Figure 1; h_c is the distance between both reference perfectly smooth surfaces and f_q is an adimensional EHL variable based on the radii, a sort of correction factor. Their respective formulations are developed in [13] and conclude in eq.(12).

$$h^* = h_m + h_c f_q \quad (12)$$

Such that h_m is the minimal surface separation accounting for deformation; h_c is the undeformed surface theoretical distance and f_q is the EHL adjustment geometrical factor.

Figure 1 below depicts the surface which a pair of surfaces, entering a full EHL contact suffer and their respective speeds U_1 and U_2 . The original surface separation h_c must be sufficient so it's large than the deformed asperity height (h_m), alas, the real surface separation would be the minimum surface separation (h_o). If at any point h_o is greater than h_c there will be direct contact between the surfaces.

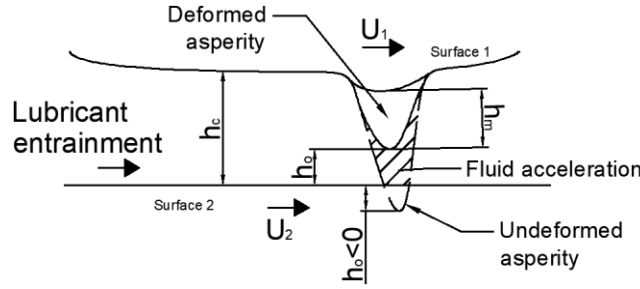


Figure 1 Traditional EHL parameter depiction

Furthermore, in the publication [12], the authors go into a lot of trouble to describe their newfound height h^* based on traditional EHL parameters, arriving at eq.(13, eq.(14 and eq.(15.

$$h_m = 3.63U^{0.68}G^{0.49}W^{-0.073}(1 - e^{-0.68k})R'_x | k = 1.03 \left(\frac{R'_y}{R'_x} \right)^{\frac{2}{\pi}} \quad (13)$$

$$h_c = 2.69U^{0.67}G^{0.53}W^{-0.067}(1 - 0.61e^{-0.73k})R'_x | k = 1.03 \left(\frac{R'_y}{R'_x} \right)^{\frac{2}{\pi}} \quad (14)$$

$$f_q = \left(\frac{R'_{x,a}}{R'_{x,b}} \right)^{\alpha_{EHL}} \frac{1 - \gamma_1 e^{-\gamma_2 \left(\frac{R'_{y,a}}{R'_{x,a}} \right)^{\gamma_3}}}{1 - \gamma_1 e^{-\gamma_2 \left(\frac{R'_{y,b}}{R'_{x,b}} \right)^{\gamma_3}}} \quad (15)$$

In both equations above (eq.(13) and eq.(14)) U represents the dimensionless speed parameter, G the dimensionless material parameter, W the dimensionless load parameter, R'_x is the effective radius in the entrainment direction and R'_y is the effective radius in the perpendicular direction. Finally, in eq.(15) $R'_{x,a}$ is the effective asperity radius in the entrainment direction; $R'_{y,a}$ is the effective asperity radius in the perpendicular direction, $R'_{y,b}$ is the effective macro geometry radius in the entrainment direction, $R'_{x,b}$ is the effective macro geometry radius in the entrainment direction, α_{EHL} is the EHL geometric coefficient and a series of EHL coefficients are depicted as γ_1 , γ_2 and γ_3 . The values of all four coefficients are shown below in Table 1:

Table 1 Adimensional EHL coefficients

Surface roughness direction	α_{EHL} (-)	γ_1 (-)	γ_2 (-)	γ_3 (-)
Isotropic & transversal	1.134 - X	0.61	0.75	2/ π
Longitudinal	1.146 - X	1	1.23	2/3

This does not necessarily agree the hypothesis proposed in [6], where the fluid film thickness was theorized to decrease with an increasing SRR. When modifying the general formulation to gears, the radius $R'_{y,b}$ and R'_y are ∞ since the gears in the entrainment direction represent a circumference centred in the pressure line, but in the perpendicular direction, they are but a flat line, thus having an infinite radius, alas, the equations can be simplified. An added benefit of this formulation is the removal of the film thickness as an independent variable when considering micro pitting, as described previously in [14].

This section contains the details to accurately predict if there is a full EHL or some other lubrication regime.

2.4. Pressure across the oil film

Reynold's equations relies on the thickness of the lubricant film being far smaller than its length, which, as per the reference [15], this tends to agree with the CFD simulations, however, it can present issues and uncertainties when the surface has a high roughness, which, is inherently present in ground or honed gears, more so in powder metal gears, where the surface roughness is more pronounced as seen in [16], [17] and [18] amongst others.

Reynold's equation cannot be considered for this application since it assumes the pressure distribution through the height of the film thickness is uniform, which, since the beginning was assumed to be false. Furthermore, it also assumes the thickness of the fluid layer is much smaller than its two counterparts in space, which, given the problem configuration is not necessarily true since a gear width might only be a few times the teeth height in some instances and thus, in the approximation phase of two flanks, the fluid film thickness can be comparable in magnitude to the other two dimensions found in space.

Another key element when discarding this version of applied fluid dynamics comes from the reference [19]. In this PhD thesis, the author explains that a key element in determining the friction coefficient is the surface boundary layer. On top of that, said surface boundary layer is strongly dependant on the chemical composition of the lubricant and pre-existing conditions, namely, surface roughness after different gear manufacturing operations, which included green shaving; power honing and grinding, alas, no assumptions about the lubricant can be made, such as the ones in Reynold's equations.

This section makes an argument for employing Navier-Stokes equations rather Reynold's equation.

3. Implementation

This section adapts the formulas and proposal from the literature review in section 2 for this application. Firstly, the general model's functioning is described in section 3.1. The implementation of the Navier-Stokes equations to describe the effect of lubricant pressure on both surfaces are shown in section 0 and the general model outputs are shown in section 3.3.

3.1. Model inner workings

The model proceeds to estimate the friction coefficient followed by the lubrication regime, which then result in one of two solvers. If a full EHL regime is estimated the surfaces will not be in contact and a thin layer of fluid with a minimum thickness of $h_o = h^*$ is implemented, which, then yields a pressure field across the fluid acting on the surfaces. The sliding and rolling forces are then allocated uniformly across the surface of each gear.

If however, the lubrication equations suggest there is mixed lubrication (ML) or boundary lubrication (BL), a numerical solver based on the rough contact model is implemented. This solver lowers both surfaces into each other and using the compliance matrix estimates stress whilst simultaneously applying the fluid

pressure due to the Navier-Stokes solution. Said stress and pressure are integrated across the entire line contact until the contact force converges. This model's operation is depicted below in Figure 2.

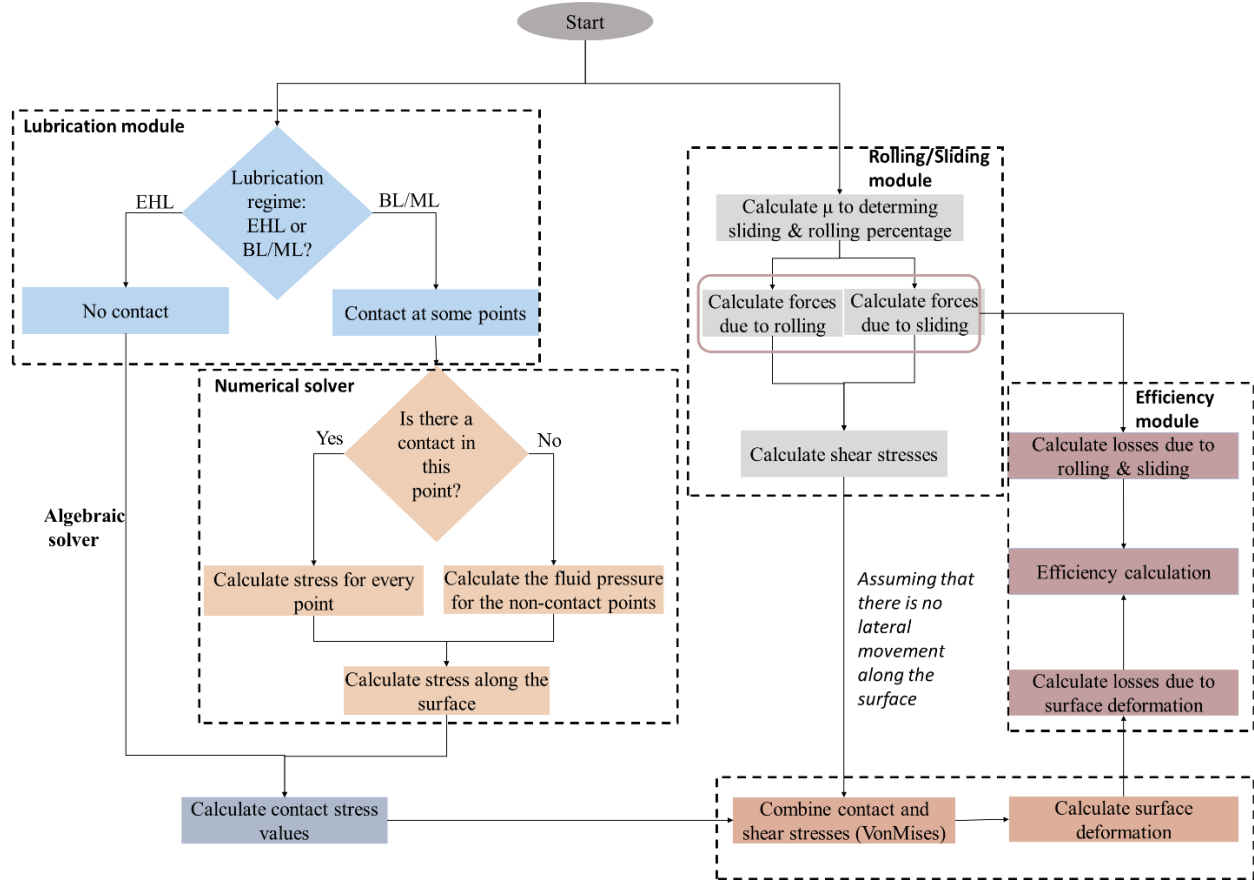


Figure 2 Model overview, decision logic & outputs

Regardless of the solver, the model then proceeds to calculate the efficiency of the contact as well as other outputs such as transferred torque by the driven gear with the formula in eq.(16).

$$M_2 = \frac{M_1 \omega_1}{\omega_2} \eta \quad (16)$$

Where M_2 is the output torque, M_1 is the input torque, ω_1 is the input rotational speed, ω_2 is the output rotational speed and η is the efficiency.

3.1.1. Efficiency

Windage and churning losses, although they were reviewed, were not implemented in this model since they are themselves external to a pair of gears meshing. The sliding and rolling resistance losses were described as eq.(17 and eq.(18).

$$P_\mu = F_s V_s \quad (17)$$

$$P_{roll} = F_r V_e \quad (18)$$

Where P_μ is the power lost due to friction with F_s standing for the friction force, V_s the sliding velocity, and P_{roll} as the power lost due to the rolling resistance, which is in turn composed of F_r as the rolling resistance and V_e being the entrainment speed.

The theoretical formulation of the power lost to deformation with a surface integral was substituted in the code with a multiplication of stress and deformation at every point in the line measurements, with a squared differential with side a to concord with the rough deformation contact model as depicted in eq.(19). Finally, the efficiency is thus calculated as eq.(20).

$$P_{si} = \frac{\iint \sigma \delta \cdot ds}{T} \rightarrow \frac{\sigma \delta_{def} a^2}{T} \quad (19)$$

$$\eta = \frac{M_1 \omega_1 - P_\mu - P_r - P_{s1} - P_{s2}}{M_1 \omega_1} \quad (20)$$

Where P_{si} are the losses due to surface deformation of each surface, σ is the Von Misses surface stress, which can be elastic or plastic, δ_{def} is the deformation depth at every point, T is the period of rotation of the gears and a^2 being the surface of a square differential.

The novelty introduced in this section is the reformulation of efficiency parameters towards numerical solver with differentials instead of integrals, making the code quicker to run.

3.1.2. Shear stress & fluid pressure allocation

In the 2D deformable, rough line contact the fluid pressure influence and other forces acting on the surface is allocated differently depending on the lubrication regime.

When there is full EHL the pressure of the fluid is applied on both surfaces following the Navier-Stokes solution, as such $\sigma = P(r, \theta, \omega_1, \omega_2, \mu, \rho, R_b, h)$ for every point of the line contact of each surface, therefore, the variation of the pressure across the fluid pressure is considered. The shear stress due to rolling and sliding are then divided even across the entire line contact, as the fluid acts equally on the entire surface.

In BL or ML cases, the numerical solver already accounts for the pressure effect of the Navier-Stokes solution. If there is contact between surfaces, points where both surfaces, the formulation for allocating sliding and rolling resistance varies, such that the rolling resistance is allocated to said points, as for rolling resistance there needs to be surface engagement and the sliding forces are slightly modified to accommodate metal to metal contact, therefore, the surface stress follows the allocation logic and convergence eq.(21). Ensuring thus that the macroscopically calculated forces are verified by the model, since those are the precise formulations.

The novelty of this section is the precise allocation of the different forces, allowing to study microscopic effects at every point of both line surfaces whilst converging towards the macro-level values which from section 0 are known to be extremely precise.

$$\begin{cases} F_m = \sum \mu_m a^2 w_{con} \\ F_{s_no} = \sum \mu a^2 w_{no} \\ F_s = F_{s_no} + F_m \end{cases} \quad (21)$$

Where F_m is the sliding resistance from a metal-to-metal contact, along with the metal-to-metal friction coefficient, μ_m and w_{con} is the load experienced by every differential in contact with the opposing surface. On the other hand F_{s_no} represents the friction due to the fluid action and it's entirely dependent on the square differential size, a , the fluid's friction coefficient μ and the load in differentials which are not in contact with the other surface. Ensuring thus that the macroscopically calculated forces are verified by the model, since those are the precise formulations.

3.2. Navier-Stokes application

Following traditional Involute straight-gear design, a flank, at any point, can be described as the circumference with radius R_i and centre along the pressure line, with an inclination α with regards to the perpendicular of the line connecting both gear centres, as seen in Figure 3, as such, the Navier-Stokes equation can be solved in a cylindrical base.

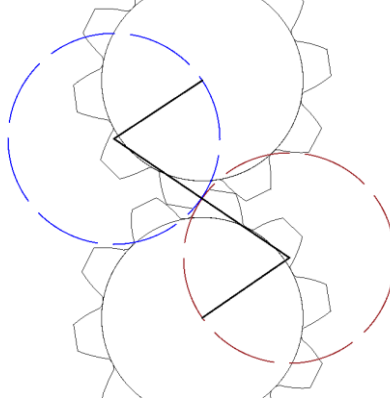


Figure 3 Gear tooth profile representation

An added benefit on considering line contacts in the middle of the gear flank rather than close to the tip is that the effects of tip reliefs can be largely simplified. As detailed in [20], a tip relief can squeeze lubricant out of the contact, leading to a fluid film height reduction and artificially altering the contour conditions so that a rougher contact between the surfaces exists and the lubricated contact hypothesis is no longer applicable. The fluid continuity equation can be written as eq.(22).

$$\frac{1}{r} \frac{\partial(r u_r)}{\partial r} + \frac{1}{r} \frac{\partial u_\theta}{\partial \theta} + \frac{\partial u_z}{\partial z} = - \frac{\partial \rho}{\partial t} \quad (22)$$

Where r is the radial direction value, θ is the angle coordinate, z is the vertical coordinate, ρ is the fluid density, t is time, u_r , u_θ and u_z are the fluid velocities in each of the respective directions. Alas, the Navier-Stokes equations become eq.(23).

$$\begin{aligned} \ddot{r}: \rho \left(\frac{\partial u_r}{\partial t} + u_r \frac{\partial u_r}{\partial r} + \frac{u_\theta}{r} \frac{\partial u_r}{\partial \theta} - \frac{u_\theta^2}{r} + u_z \frac{\partial u_r}{\partial z} \right) &= - \frac{\partial P}{\partial r} + \rho g_r + \mu \left[\frac{1}{r} \frac{\partial}{\partial r} \left(r \frac{\partial u_r}{\partial r} \right) - \frac{u_r}{r^2} + \frac{1}{r^2} \frac{\partial^2 u_r}{\partial \theta^2} - \frac{1}{r^2} \frac{\partial u_\theta}{\partial \theta} + \frac{\partial^2 u_r}{\partial z^2} \right] \\ \ddot{\theta}: \rho \left(\frac{\partial u_\theta}{\partial t} + u_r \frac{\partial u_\theta}{\partial r} + \frac{u_\theta}{r} \frac{\partial u_\theta}{\partial \theta} - \frac{u_r u_\theta}{r} + u_z \frac{\partial u_\theta}{\partial z} \right) &= - \frac{\partial P}{\partial \theta} + \rho g_\theta + \mu \left[\frac{1}{r} \frac{\partial}{\partial r} \left(r \frac{\partial u_\theta}{\partial r} \right) - \frac{u_\theta}{r^2} + \frac{1}{r^2} \frac{\partial^2 u_\theta}{\partial \theta^2} - \frac{2}{r^2} \frac{\partial u_r}{\partial \theta} + \frac{\partial^2 u_\theta}{\partial z^2} \right] \\ \ddot{z}: \rho \left(\frac{\partial u_z}{\partial t} + u_r \frac{\partial u_z}{\partial r} + \frac{u_\theta}{r} \frac{\partial u_z}{\partial \theta} - \frac{u_\theta}{r} \frac{\partial u_z}{\partial \theta} + u_z \frac{\partial u_z}{\partial z} \right) &= - \frac{\partial P}{\partial z} + \rho g_z + \mu \left[\frac{1}{r} \frac{\partial}{\partial r} \left(r \frac{\partial u_z}{\partial r} \right) + \frac{1}{r^2} \frac{\partial^2 u_z}{\partial \theta^2} + \frac{\partial^2 u_z}{\partial z^2} \right] \end{aligned} \quad (23)$$

Where p is the fluid film pressure, x and y are the width and length respectively, h is the flim thickness thickness, μ is the fluid viscosity, ρ is a fluid density, u, v, w are the bounding body velocities in all three dimensions of space respectively and the subscripts a and b represent each of the moving bodies. The simplifications taken for granted when solving these equations are shown in eq.(24, eq.(25, eq.(26, eq.(27 and eq.(28).

$$u_z = 0 \quad (24)$$

$$\frac{\partial^i u_r}{\partial z^i} = 0 \mid i \in \mathbb{N} \quad (25)$$

$$\frac{\partial u_i}{\partial t} = 0 \mid i \in [\vec{r}, \vec{\theta}, \vec{z}] \quad (26)$$

$$\frac{\partial^i u_\theta}{\partial z^i} = 0 \mid i \in \mathbb{N} \quad (27)$$

$$\vec{g} = \begin{bmatrix} 0 \\ 3 \times 1 \end{bmatrix} \quad (28)$$

These simplifications imply the fluid does not move across the flank of the tooth, which, as it's well known, is inherently false, however, this allows to model the movement of the fluid across the meshing of the flanks more simply. Considering the velocity in both \vec{r} and $\vec{\theta}$ to be independent from \vec{z} allows for a fully decoupled two-dimensional model along the \vec{r} and $\vec{\theta}$ directions (see *Figure 5*), which, represents uniform pressure across the fluid “layers”, thus resulting in varying pressures for two points in different z coordinates but same \vec{r} and $\vec{\theta}$, thus, respecting the pseudo-three-dimensional problem configuration proposed.

Considering the fluid velocity variation to be dependent of the angle position as well as the radius allows for the computation of the fluid compression as the points in the gear surface move closer together, thus 2 points in the same circumference to have different pressures as they would be in different angles and therefore, the fluid will not behave as laminar throughout the model, which, would be a poor definition.

The effects of gravity have been disregarded throughout the model, since, at its core it will operate with the film thickness provided by the corresponding EHL model.

Time effects have been disregarded since it would overcomplicate the model and increase the computational cost without adding too much information, since the model itself works by converging a set of stationary events.

To further solve the model, a velocity field is required, and for such, being consistent with the previously listed simplifications, the velocity field has been assumed to be turbulent and therefore, it presents a parabolic distribution through the fluid height, represented below in *Figure 4*.

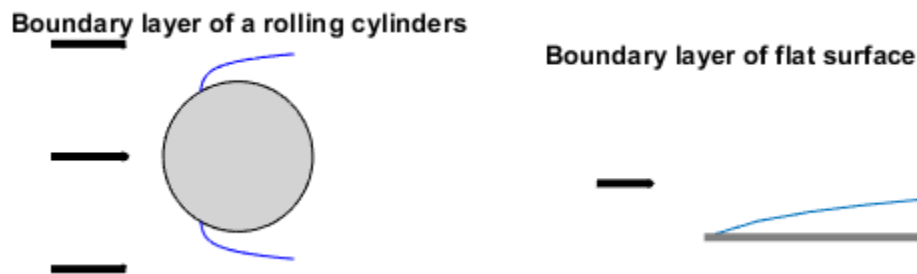


Figure 4 Boundary layer representation

This is applicable when a thick enough fluid layer (fluid total thickness is greater than the boundary layer height) lies on the gear's surface, which can be obtained via normal dipping techniques; jet lubrication or full submersion. Different lubrication techniques are discussed in [21]. In this work the different effects of lubrication and their effect on scuffing is discussed. The conclusion is that mist nor dip lubrication are sufficient to prevent scuffing, where, overall, mist lubrication is blatantly insufficient for the load cases presented in the report. Jet lubrication was found to have a strong correlation with load and consequently with flow rate. It also showed that jet velocity is more important than volumetric flow rate when preventing scuffing.

The fluid height, at any point of the fluid can be described exclusively as a function of the EHL film thickness (h_o) and the angle in cylindrical coordinates (with the origin aligned with one of the roller's main axes) can be found in eq(29) and depicted in *Figure 5*.

$$h = h_o + (1 - \cos \theta)(r_1 + r_2) \quad (29)$$

Such that h is the separation at any radial-angular coordinate pair, r_1 is the equivalent radius of the driving flank and r_2 is the equivalent radius of the coast flank.

Navier Stokes stand-in variables

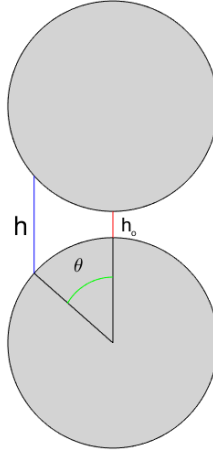


Figure 5 Navier-Stokes stand in contour variables

As such, the fluid velocity can be rewritten as a function of height and therefore, inherently, θ and the radius, thus, the following system of equations can be solved from eq.(30).

$$\begin{cases} v(h) = A_{fluid}h^2 + B_{fluid}^2h + C_{fluid} \\ v(\theta = 0, r = r_2) = \omega_2r_2 \\ v(\theta = 0, r = r_1) = \omega_1r_1 \end{cases} \quad (30)$$

Where A, B and C are the coefficients to be calculated, ω_i is the radial speed of the gear tooth (for the driving and driven gears 1 and 2 respectively). To solve the model, it is imperative to rely on a variable denoted as u_∞ which is widely regarded as the fluid velocity far away from the working surfaces and the boundary layer thereby generated. Hence stability in time and space is achieved.

Since both A and B are linearly dependent on u_∞ they would be remarkably sensible to it, alas, u_∞ is a key parameter. A commonly accepted simplification assumes this velocity to be 0 or in moving reference, the properties of said base e.g. a transmission solidary to a moving vehicle. Another reasonable assumption would be for u_∞ to be the velocity extracted from solving Bernoulli's equation for any fluid line stemming from a coolant pump considering energy losses due to the changes in surface area and vorticity of the fluid when passing through the gears.

Another, simpler way of approximating u_∞ is by applying Bernoulli's equation backwards once the fluid's pressure field is fully characterized in the meshing point.

Either way, accepting, this definition of the fluid velocity represents u_θ , the continuity equation yields the velocity distribution as a function of the radius eq.(31). If in turn, $u_r = 0 \forall r$, then

$u_r = 0 \forall r \Leftrightarrow C = 0$, the velocity field of the fluid at any point within the boundary layer can be described as eq.(32).

$$u_r = -\frac{1}{r}(r_1 + r_2)(2hA_{fluid}\sin\theta + B_{fluid}\sin\theta)(r + D_{fluid}) - C_{fluid} \quad (31)$$

$$\begin{bmatrix} u_r \\ u_\theta \\ u_z \end{bmatrix} = \begin{bmatrix} -\frac{1}{r}(r_1 + r_2)(2hA_{fluid}\sin\theta + B_{fluid}\sin\theta)(r + D) \\ A_{fluid}h^2 + B_{fluid}^2h + \omega_2r_2 \\ 0 \end{bmatrix} \Big| \begin{cases} A = \frac{4}{(r_2 + h_o)^2} \left(\frac{\omega_1r_1 + \omega_2r_2}{2} - u_\infty \right) \\ B = \frac{4u_\infty - (\omega_1r_1 + 3\omega_2r_2)}{r_2 + h_o} \end{cases} \quad (32)$$

Solving for D in turn (the integration constant) could be done so by calculating the boundary layer for a rotating cylinder eq.(33).

$$u_r(r = \delta_{BL}) = u_\infty \quad (33)$$

Where δ_{BL} is the height of the boundary layer at any point of the gear's flank profile and u_∞ is the velocity of the undisturbed fluid. The boundary layer has been approximated by several renowned authors such as Reynold, Parndtl and Von Karman, in this algorithm, the logarithmic implementation. Alternatively, an infinitely thin layer of fluid in contact with a moving solid will always move at the wall's speed, alas, the point at which the boundary layer starts can be described as the point where there is solidarity in movement, there is no radial component since the wall has exclusively movement in the $\vec{\theta}$ direction, alas, solving for D we get, assuming the boundary layer starts at the root of the flank since above there is an existing vorticity from the previous tooth eq.(34, eq.(35 and eq.(36).

$$\theta_{pass} = \frac{2\pi}{z} \quad (34)$$

$$R_b = mz * \cos\alpha \quad (35)$$

$$\vec{u}(P) = \begin{bmatrix} u_r = 0 \\ u_\theta = u_{wall} \end{bmatrix} \Leftrightarrow D = -R_b \quad (36)$$

Where θ_{pass} is the gear pitch, R_b is the base diameter with module m , number of teeth z and pressure angle α . Therefore, finally the Navier-Stokes equations can be solved to calculate the pressure field of the fluid, only in the \vec{r} direction since the inevitable consequence of decoupling the \vec{z} direction yields eq.(37).

$$\frac{\partial P}{\partial z} = 0 \quad (37)$$

The novelty introduced by this section is the approximation for the Navier-Stokes solution for this configuration, with a static approach and disregarding one of the 3 physical dimensions, whilst being able to fully characterize the development of the lubrication boundary layer along the full length of the profile with minimum computational cost.

3.3. Model outputs

As such the model can calculate the surface deformations of the contact between two gear teeth, both within the contact, elastic, and plastic deformation, and after the contact, permanent or plastic deformation. From the lubrication formulations it can also output the oil film thickness and stemming from there, the pressure distribution across the oil film. Finally, other than efficiency and torque of the driven gear, it can estimate the efficiency of the gears meshing on top of the convergence history.

The novelty of this section is the consolidation of all losses and the breakdown on how they each affect the meshing efficiency whilst also being extremely efficient with the resources used.

4. Evaluation

Each module of the model was tested independently to allow for refinement and optimization.

4.1. Dry contact module evaluation

The contact module was tested in dry conditions with randomly generated surfaces, as in Figure 6 below:

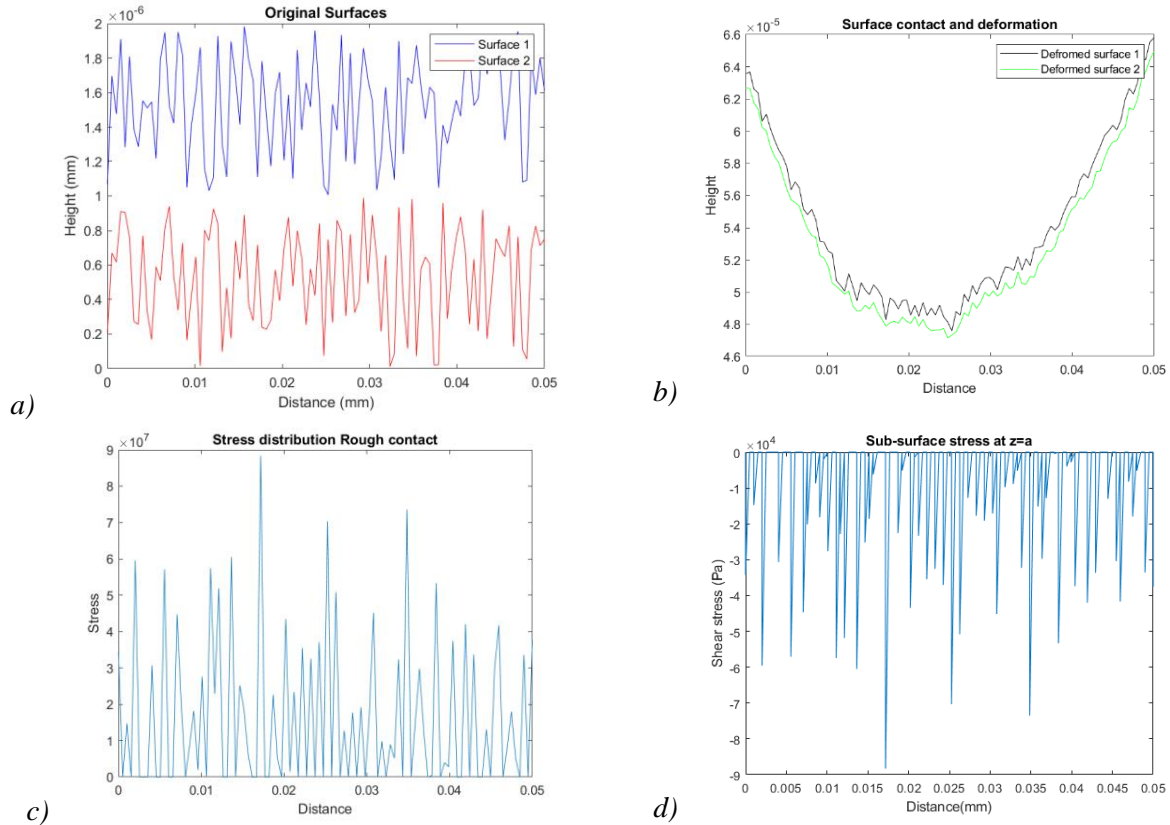


Figure 6: a) Starting randomly generated surfaces (top left) b) Deformation of the randomly generated surfaces (top right) c) Contact stress of the randomly generated surfaces (bottom left) d) Sub-surface stress of the randomly generated surfaces (bottom right)

For all tests where a real measurement was used, the surface roughness measurement were taken with a MarSurf GD 120 with a $1\mu\text{m}$ radius tip and a cone angle of 60° .

4.2. Lubricant sensitivity evaluation

To evaluate the effect of the lubricant, a test matrix was assembled iterating through the lubricant's density and the absolute viscosity (with a real surface roughness line measurement). This model was run twice, with and without the pressure variation across the fluid film, the efficiency variations are shown below in Figure 7:

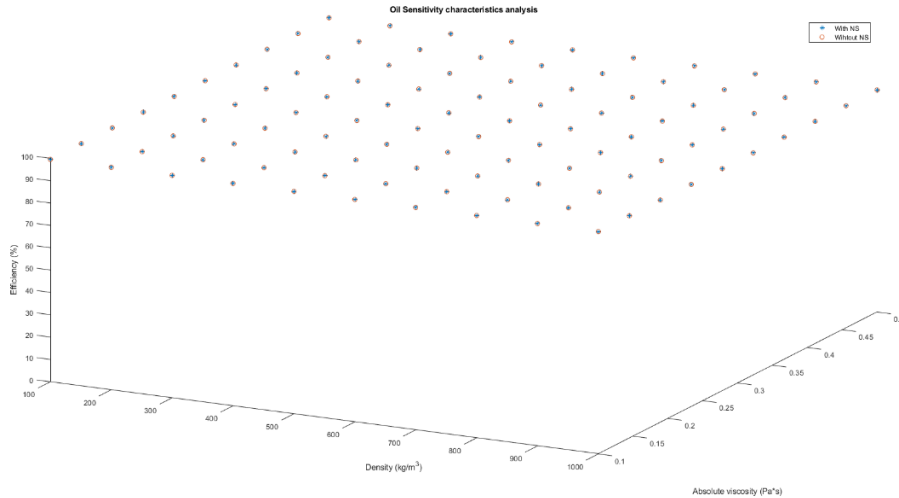


Figure 7 Lubricant sensitivity and NS validation analysis

As seen above in Figure 7, the maximum efficiency (99.4635%) coincides both with and without Navier-Stokes since the pressure contribution to the surface deformation energy is low when compared to the other contributions. Windage and churning losses also coincide and are greatly affected by the lubricant properties and drive efficiencies down enormously when more realistic lubricant properties are considered.

The pressure variation across the fluid film resulting from the Navier-Stokes solution was also studied (see **Error! Reference source not found.**):

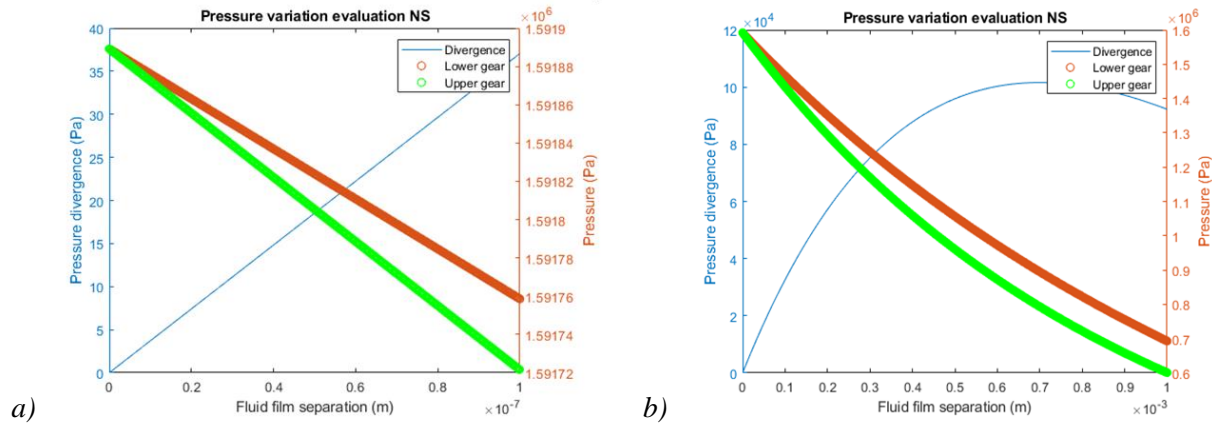


Figure 8 a) Pressure variation across thin films (left) b) Pressure variation across thick films (right)

Verifying the Reynold's approximation, the divergence in pressure across thin film is not significant whilst if the distance augments it is very relevant. The pressure variation between surfaces at 100nm is merely 37.05 Pa which compared to the 1.59 MPa the surface is under, is insignificant. In this case, for gear teeth with an equivalent circumference radius below 6mm the maximum divergence is of 16% between both surfaces, thus, the pressure variation is significant but this configuration escapes Reynold's definition since, the height is not significantly smaller than the other dimensions and said pressure loss is due to the turbulence and vorticity of the fluid.

4.3. Real surface damage evaluation

Finally, the model was tested with a real surface measurement from a region with prominent surface damage. This measurement was mirrored to create both contact surfaces. The model was then set up with the following parameters presented in Table 2:

Table 2 Input variables for validation run

Variable	Value	Units	Variable	Value	Units
Module	1.3	mm	Elastic limit 2	235	MPa
Pressure angle	20	deg	Bulk temperature 1	60	K
Helix angle	30	deg	Bulk temperature 2	60	K
Number teeth 1	50	-	Lubricant conductivity	0.135	W/m/K
Number teeth 2	120	-	Lubricant heat capacity	2	J/g/K
Width 1	50	mm	Thermal conductivity 1	45	W/m/K
Width 2	50	mm	Thermal conductivity 2	45	W/m/K
Input moment	285	Nm	Lubricant density	998	Kg/m ³
Input rotational speed	3000	rpm	Lubricant load loss dependent coefficient	0.84	-
Metal-to-metal friction coefficient	0.3	-	Reference load loss dependent coefficient	0.9069	-
Young's modulus 1	210	GPa	Lubricant absolute pressure	0.0975	Pa·s
Young's modulus 2	210	GPa	Lubricant's pressure viscosity coefficient	2e-08	mm ² /N
Poisson Coefficient 1	0.3	-	Numerical error	1	%
Poisson Coefficient 2	0.3	-	Delta step	80	nm
Elastic limit 1	235	MPa			

The model predicted a 98.8% efficiency, converged in 28 iterations, with an error of 4% and a total computational time of 75 seconds. The outputs are shown below. The surface variation in 2 separate stages will also be calculated and shown, the surface under contact, allowing to for calculation of real surface deformation and the surface after contact, where the result of the plastic deformation of the surface will be outputted. Firstly, the surface deformation shown in Figure 9:

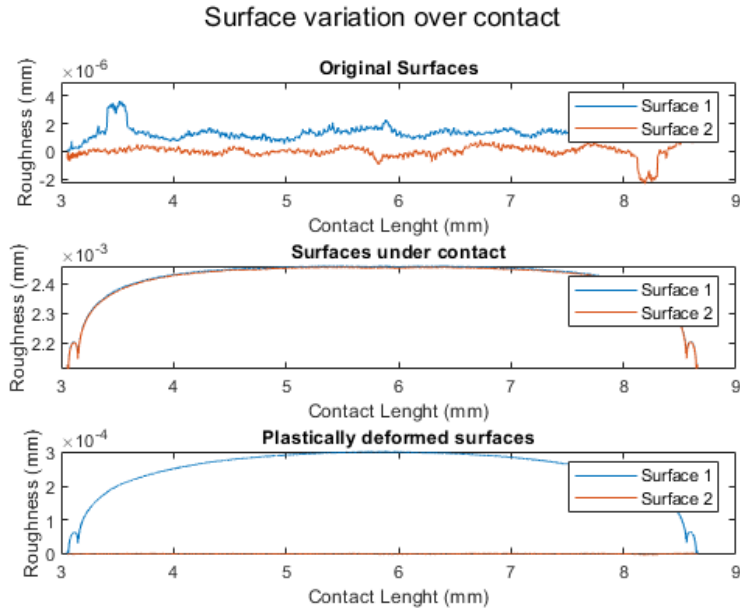


Figure 9 Sample surface module output

Then the contact stress as seen below in **Error! Reference source not found.:**

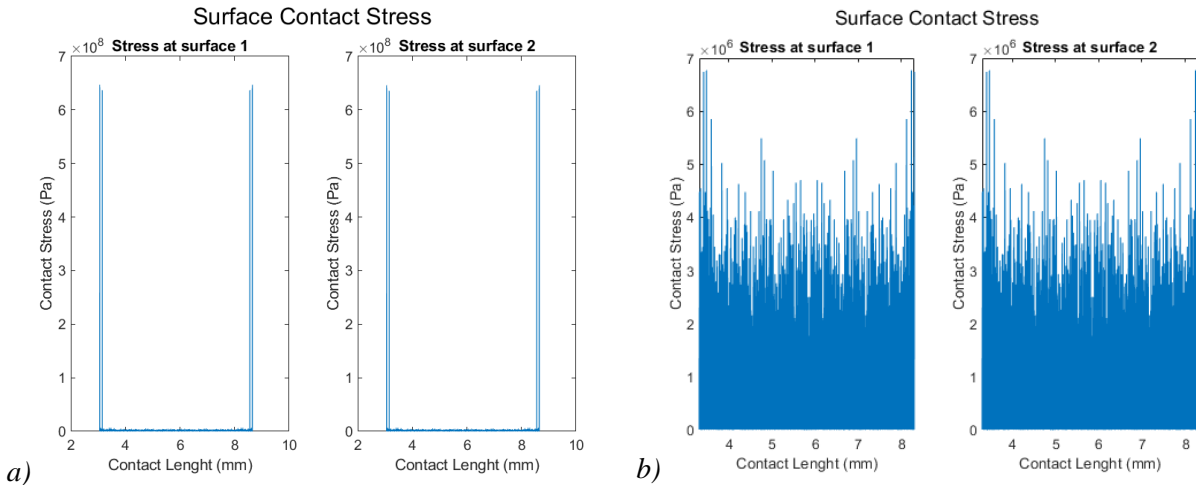


Figure 10: a) Sample contact stress output (left) b) Zoomed in stress at the centre of the contact (right)

Followed by the sub-surface stress shown in **Error! Reference source not found.:**

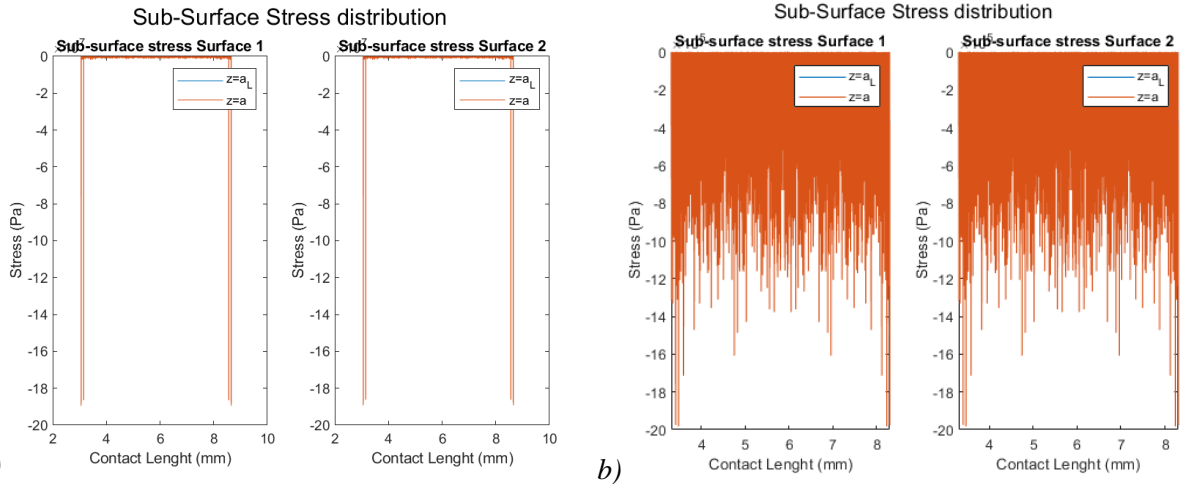


Figure 11: a) Sample sub-surface stress output (left) b) Zoomed in subsurface stress at the centre of the contact (right)

The losses distributions are also shown in **Error! Reference source not found.** below:

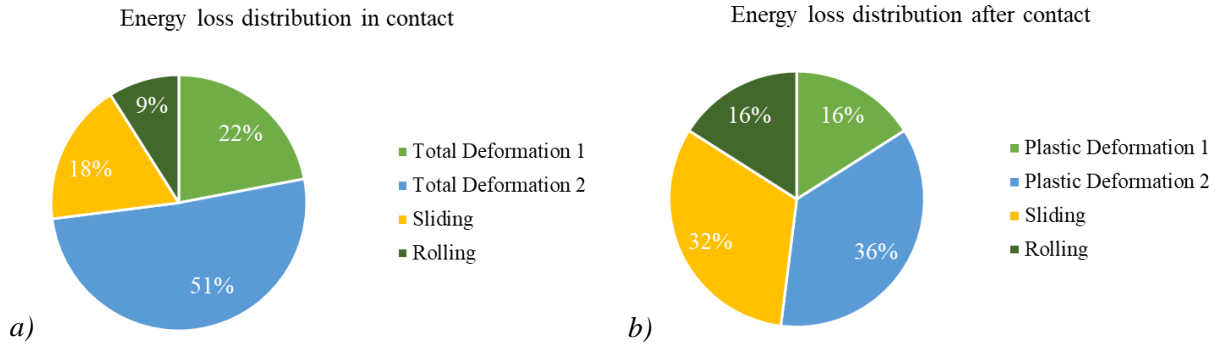


Figure 12: a) Sample energy loss distribution output upon contact (left) b) Sample permanent energy loss distribution output

Finally, the convergence history is outputted as seen below in Figure 13:

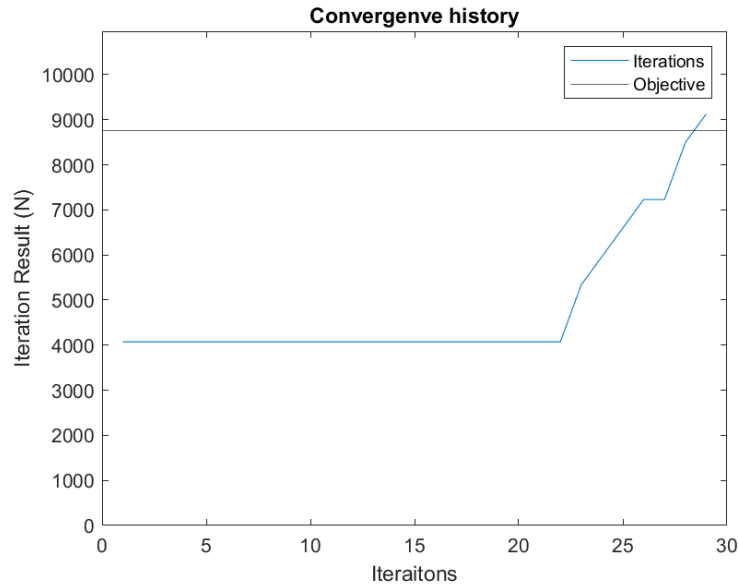


Figure 13 Sample convergence history output

5. Discussion

Considering the lubricant sensitivity evaluation presented in Section 4.2, the efficiencies are somewhat high ranging from 99.4635% to 98.4188% whereas a typical gear-to-gear transmission has an efficiency of about 98%, this is most likely due to the lubricant's density and absolute viscosity pairing since said maxima are found at the minimum density and minimum absolute viscosity, whilst, for more realistic lubricants (in both terms of viscosity and density) the efficiencies range from 98.9345% and 98.5325%, thus very close to the output shown by the various WindowsLDP¹ models of this type of gears.

It's worth noting the real absolute efficiency of the gear pairing is not known since LDP only offers approximations on different types of lubricants and therefore a small variation within the efficiency results are to be expected.

The pressure variation through the thin film thickness upon contact is largely insignificant, which, agrees with commonly accepted literature and the hypothesis of Reynold's equations.

As shown by the model in Section 4.3, there is a stress concentration in the vicinity of either surface defect (see **Error! Reference source not found.** and **Error! Reference source not found.**) which agrees with own effects of surface damage as stress concentrations, which is in turn reflected in the contacting and plastically deformed surfaces. As expected from the literature review, the sub-surface stress mimics the contact stress, and both are shown to be asymmetric and dependant on the contact and fluid pressure effects.

The losses upon the contact constitute unusable energy, since they include the elastic deformation, whilst the loss after contact are the real losses, since the elastic deformation, although unavailable, are recovered when the surface relaxes. Most of the permanent losses are divided amongst surface deformation and the sliding, see **Error! Reference source not found.** for the graphical representation.

¹ WindowsLDP is gear specific simulation software developed by Ohio State's University Gear and power transmission research laboratory.

The model at first has a constant force in the convergence history since it's the overall effect of the oil film pressure, as the surfaces are not yet in contact, whilst, later on it starts to increase as each surface runs into each other as seen in Figure 13.

6. Outlook

Clearly, the model can be further improved to accommodate a more accurate temperature module beyond the current one from essentially, adaptations of Fourier's law to better mimic the results of both ROMAX² and WindowsLDP.

The model could also be upgraded from a 2D stationary line contact model to a pseudo3D or full 3D by considering the area around the studied contact point in the case of a pseudo 3D approximation as every line in the lead direction is considered with the software running along the profile direction of the gear tooth or a full 3D by considering the gear flank as a surface body which would undoubtedly require FEM.

Perhaps it is more pressing the software be made transient and implement time-dependent factors directly into both the contact dynamics and specially in the lubrication definitions, as already discussed.

A surface generating model should also be trained with heaps of data from a myriad of surface roughness measurements before, during and after testing so a more complete picture of how the surface deforms, especially in the first cycles where running-in takes place, and thus it would be able to generate surfaces as they deform and change in real life, and then evaluating efficiency changes, helping in the design and understanding of test definition and in turn improve real-life performance of electric transmissions.

Furthermore, a refined powder metal gears module should be implemented to allow for further R&D efforts to study their applications in future transmissions, reducing material usage and associated environmental impacts

7. References

- [1] M. Sosa, "Running-in of gears- surface and efficiency transformation," KTH, Stockholm, 2017.
- [2] S. B. a. B. R. L. Xiao, "The influence of surface roughness and the contact pressure distribution on friction rolling/sliding contacts," *Tribology international*, pp. 40:4:694-698, 2007.
- [3] S. Björklund, "Elastic contacts between rough surfaces.," KTH, Stockholm, 1995.
- [4] K. Johnson, "Contact Mechanics," Cambridge University Press, Cambridge, 1987.
- [5] H. e. al, "Prediction of Mechanical Efficiency of Parallel-Axis Gear Pairs," *Journal of Mechanical Engineering* 129, pp. 58-68, 2007.
- [6] P. R. a. A. Kadiric, "The influence of side-roll ratio on the extent of micropitting damage in rolling-sliding contacts pertinent to gear applications," *Tribology Letters*, pp. 67:1-20, 2019.

² ROMAX is a power transmission specific software developed by Romax Technology Ltd.

- [7] Y. M. a. V. Myunster, "Determination of power losses in gear transmissions with rolling and sliding friction incorporated," *Mechanisms and Machine Theory*, pp. 37: 167-174, 2002.
- [8] P. M. e. al, "Gear Solutions," 15 04 2021. [Online]. Available: <https://gearsolutions.com/features/predicting-gear-sliding-losses/>.
- [9] S. W. e. al, "A Frictional Model of Partial-EHL Contacts and its Applications to Power Loss in Spur Gears," *Tribology Transactions* 34, pp. 398-407, 1991.
- [10] "Chapter 2: Overall Methodology," in *DEVELOPMENT OF A GENERALIZED MECHANICAL EFFICIENCY PREDICTION METHODOLOGY FOR GEAR PAIRS* , Columbus, Ohio State University, 2005, p. 30.
- [11] m. M. e. M.M.Khonsari, "The high pressure rheology of some simple model hydrocarbons," *Tribology International* 82, pp. 228-244, 2015.
- [12] M. B. e. R. L. Jonny Hansen, "A New Film Parameter for Rough Surface EHL Contacts with Anisotropic and Isotropic Structures," *Tribology Letters* 69:37, pp. 1-17, 2021.
- [13] J. Hansen, "Elasto-hydrodynamic film formation in heavily loaded rolling-sliding contacts," Lulea University of Technology, Gothenburg, 2021.
- [14] I.-T. a. M. M. Hui Long, "Analytical and Experimental Study of Gear Surface Micropitting due to Variable Loading," *Applied Mechanics and Materials*, pp. 750: 96-103, 2015.
- [15] M. Tomic, "Model of Thermal EHL Based on Navier-Stokes Equations: Effects of asperities and Extreme Loads," *Lulea University of Technology*, pp. 1-82, 2019.
- [16] D. S. Dizdar, "High-Performance Sintered-Steel Gears for Transmissions and Machinery: A Critical Review," *GEARTECHNOLOGY*, pp. 60-65, 2012.
- [17] X. Li, "Efficiency and wear properties of spur gears made of powder metallurgy materials," KTH Royal Institute of Technology, Stockholm, 2016.
- [18] D. G. Kotthoff, "NVH Potential of PM Gears for Electrified Drivetrains," *GEARTECHNOLOGY*, pp. 40-43, 2018.
- [19] E. Bergseth, "On tribological design in gear tooth contacts," Royal Institute of Technology, Stockholm, 2012.
- [20] H. U. Jamali, K. Sharif and H. E. a. R. Snide, "Transient EHL analysis of helical gears," in *International Gear Conference 2014*, Lyon, 2014.
- [21] R. M. Abraham, "AN EXPERIMENTAL STUDY OF SCUFFING PERFORMANCE OF A HELICAL GEAR PAIR SUBJECTED TO DIFFERENT LUBRICATION METHODS," Ohio State University, Columbus, 2014.

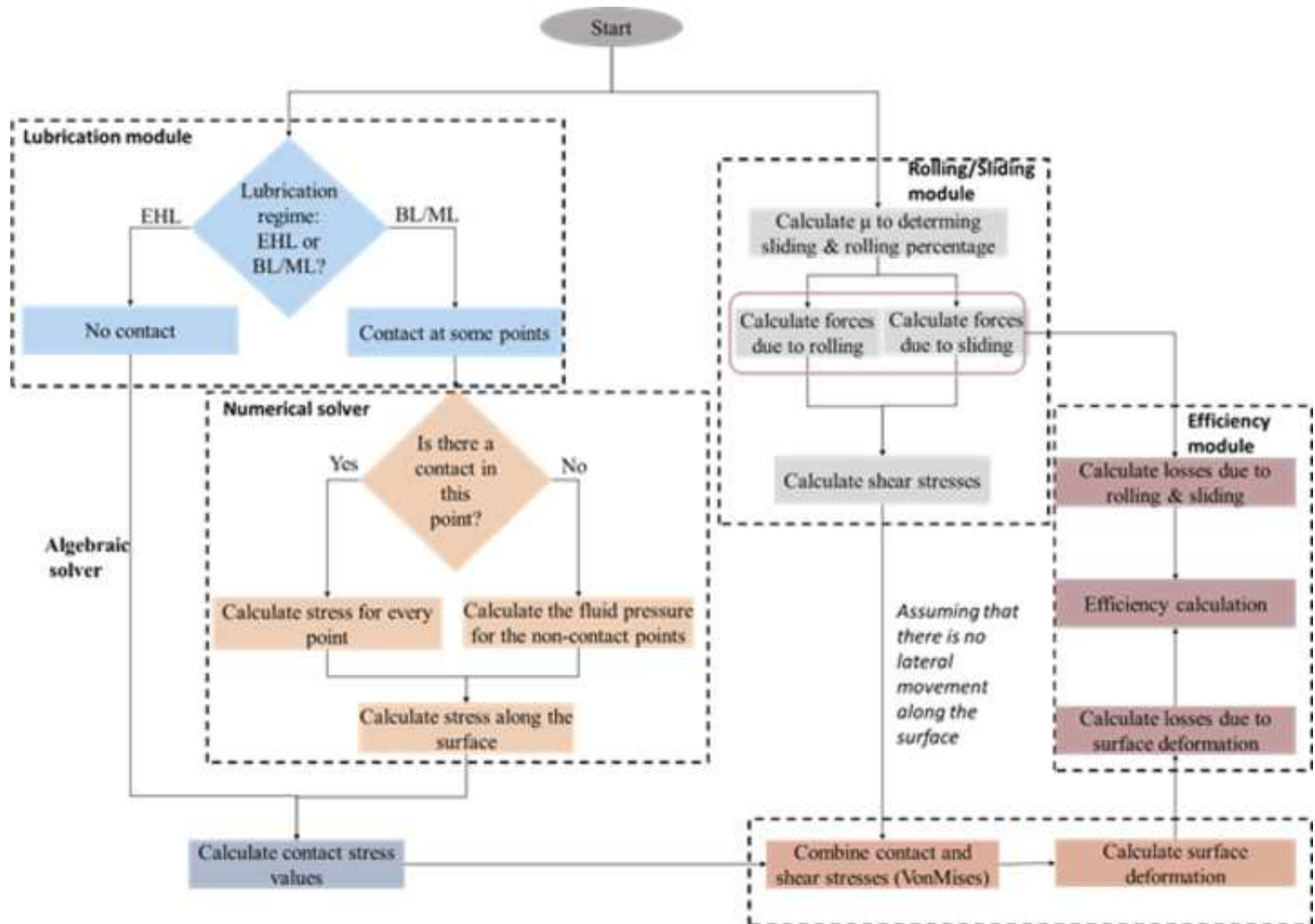
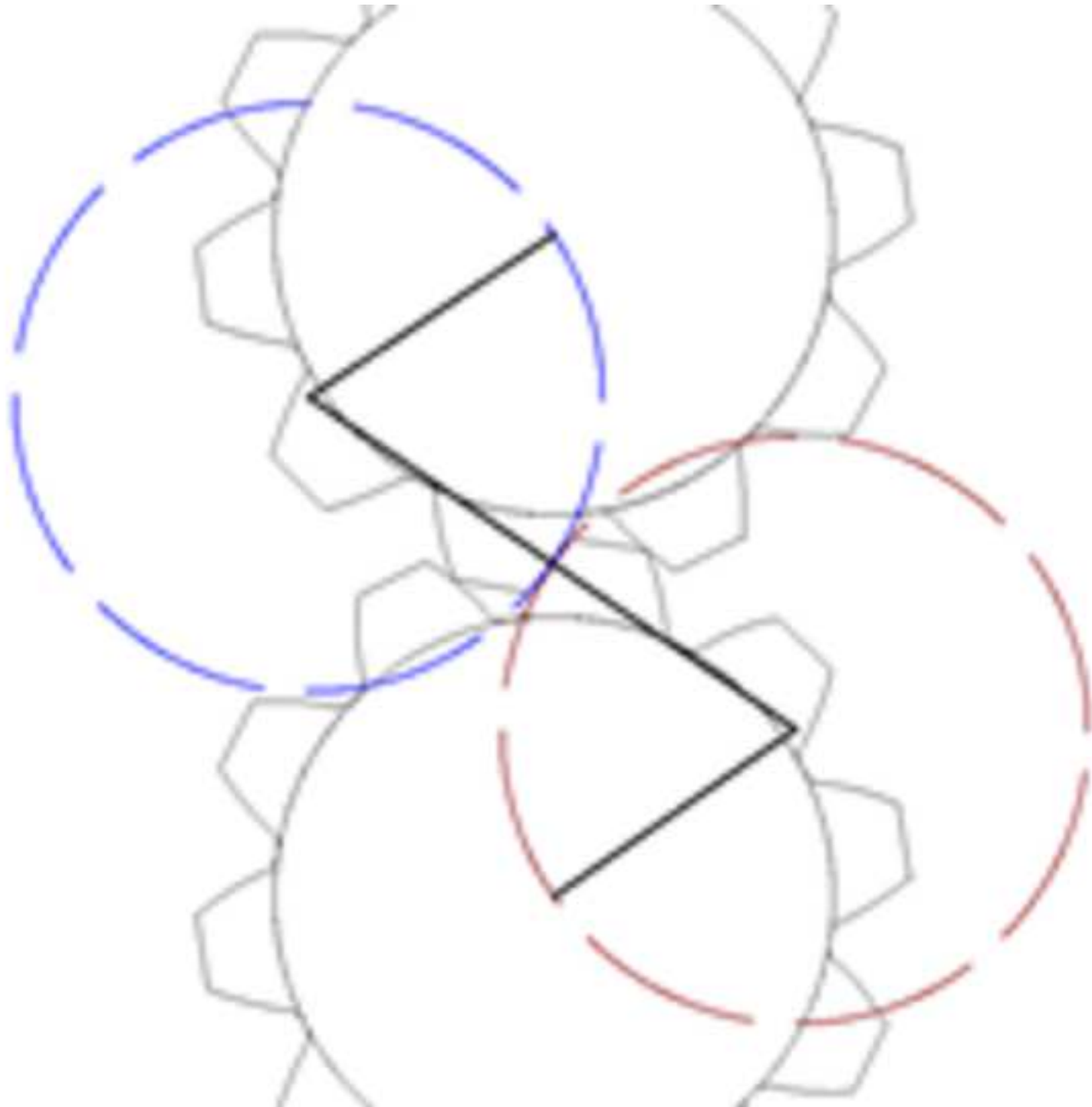
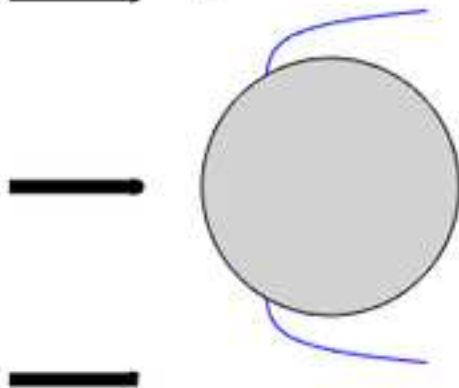


Figure 3

[Click here to access/download;Figure;Figure 3 Gear tooth profile representation.png](#)



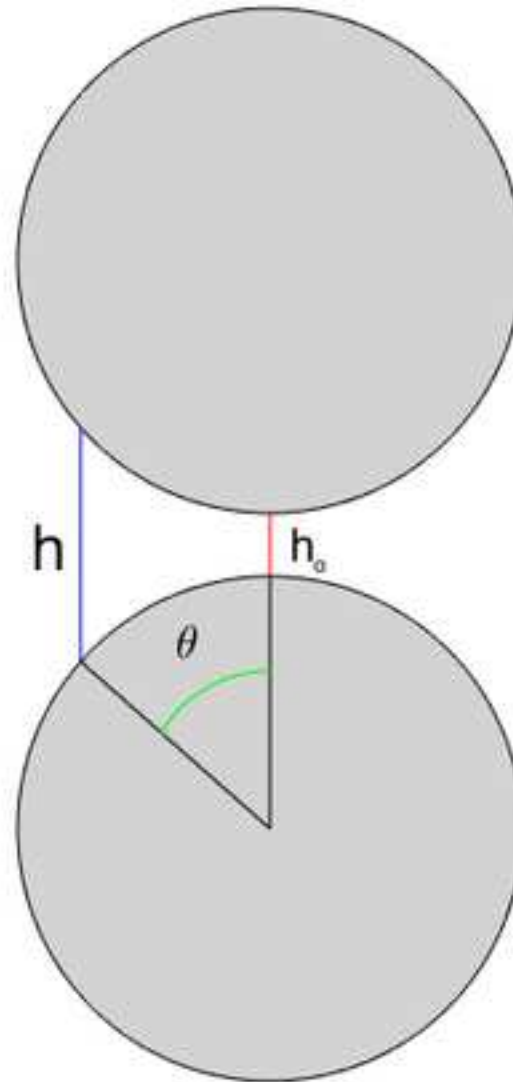
Boundary layer of a rolling cylinders

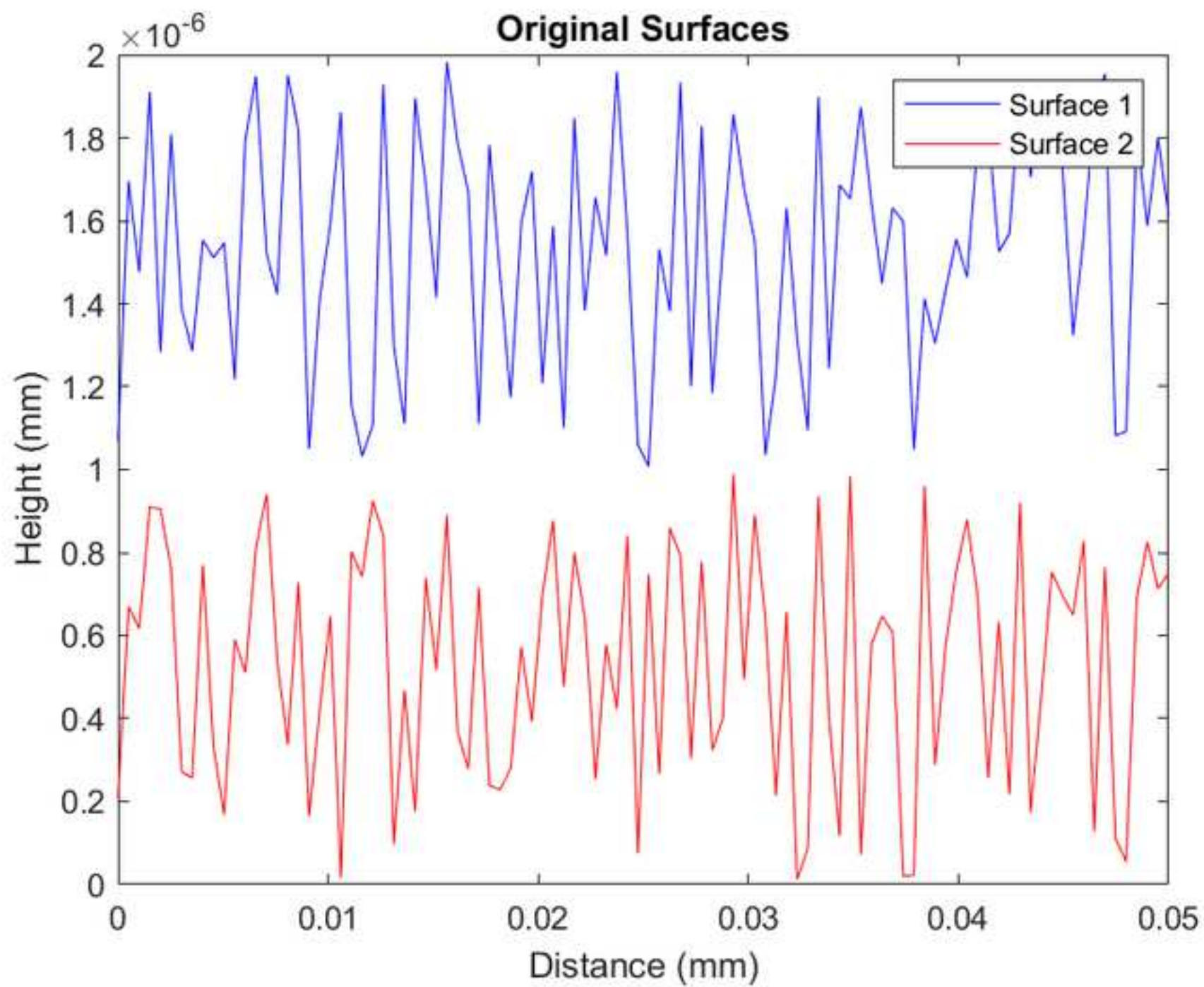


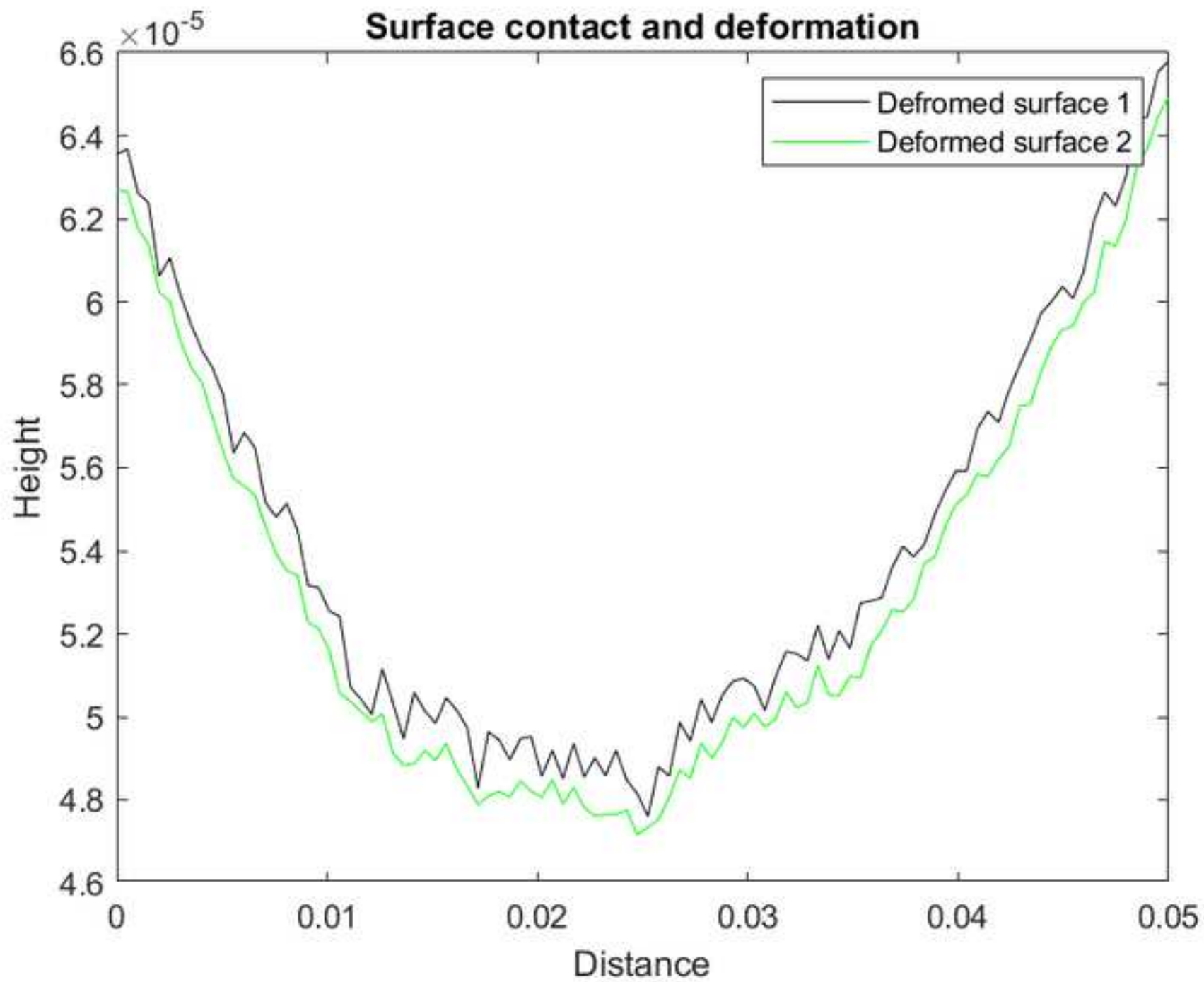
Boundary layer of flat surface

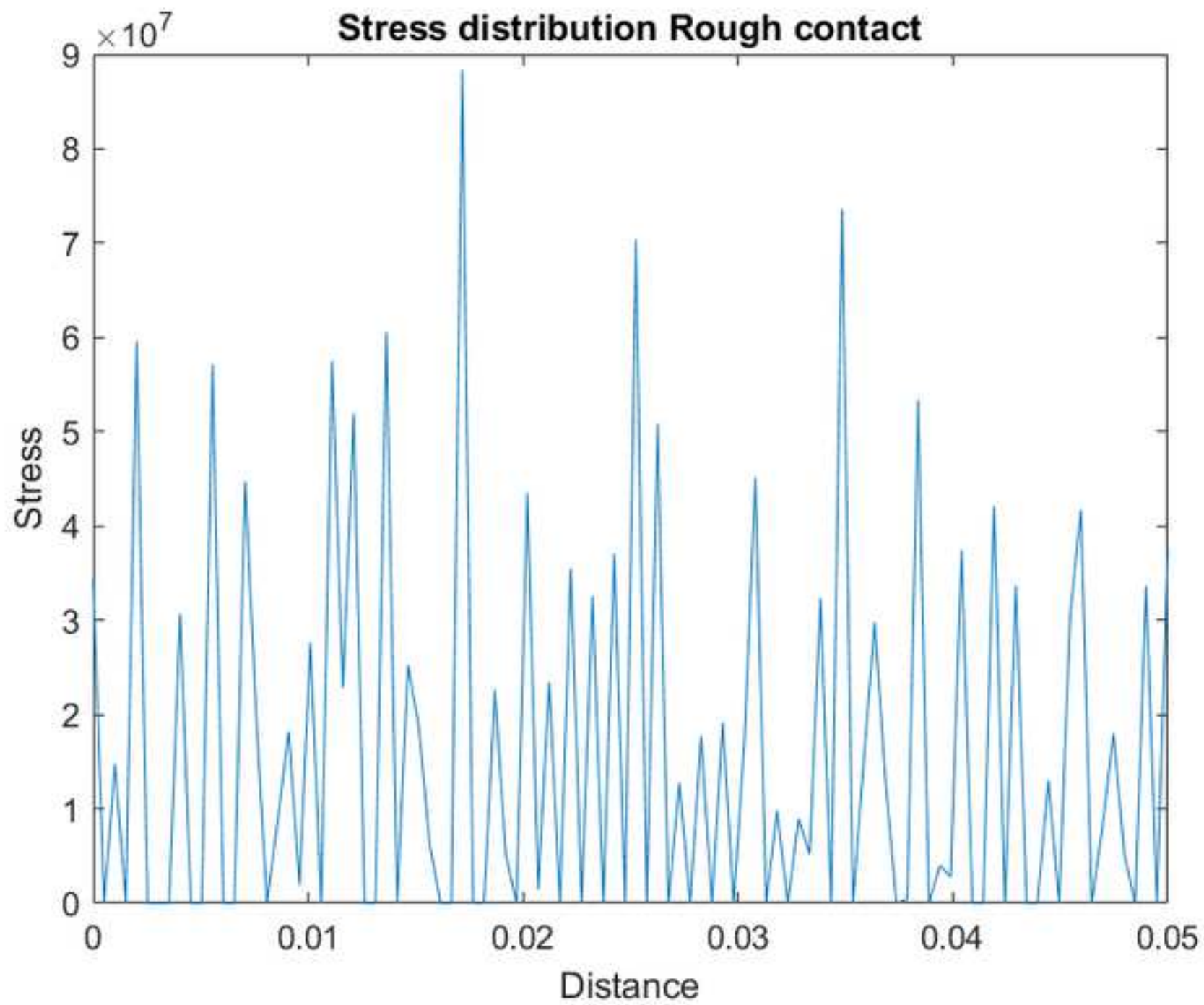


Navier Stokes stand-in variables









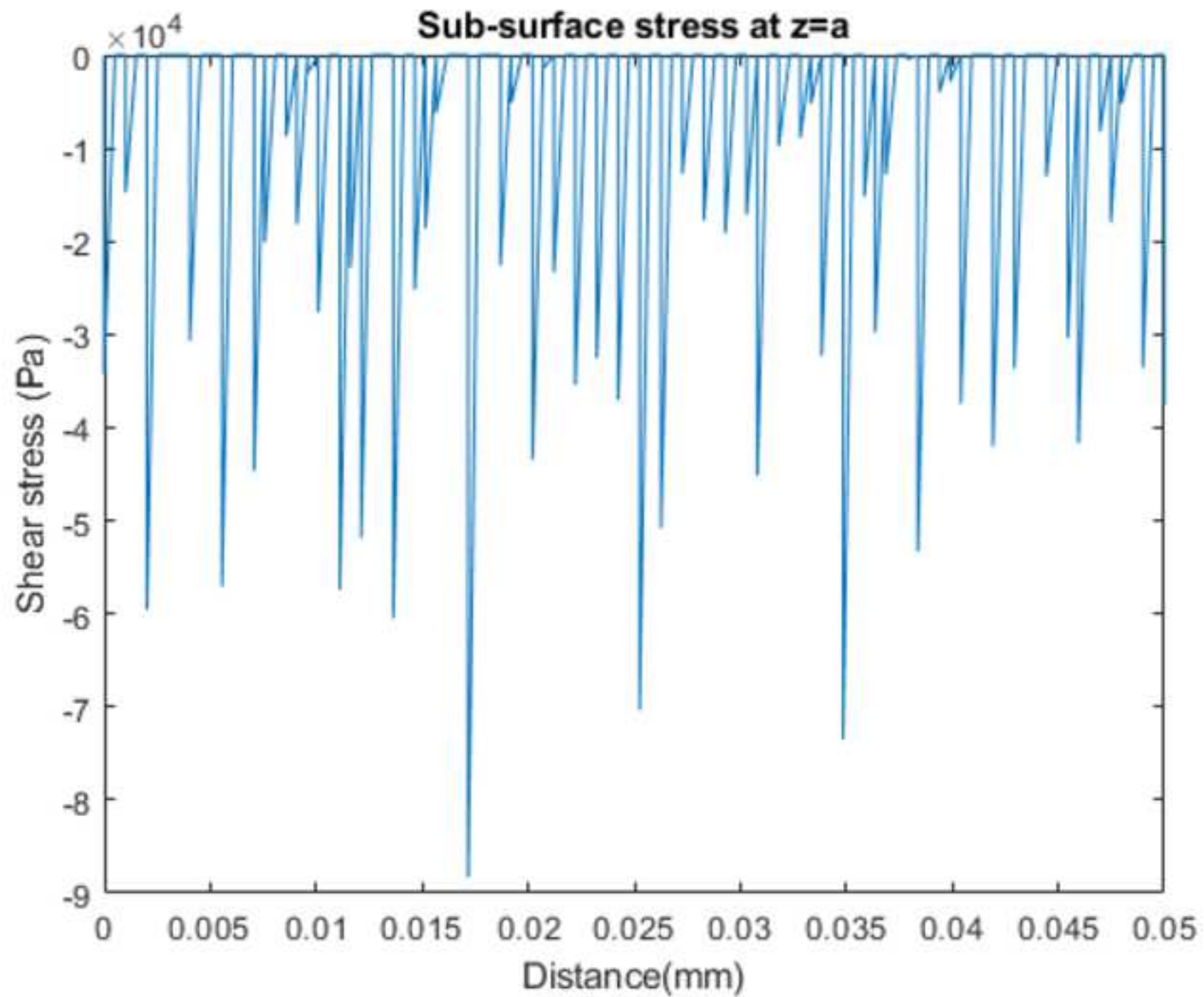
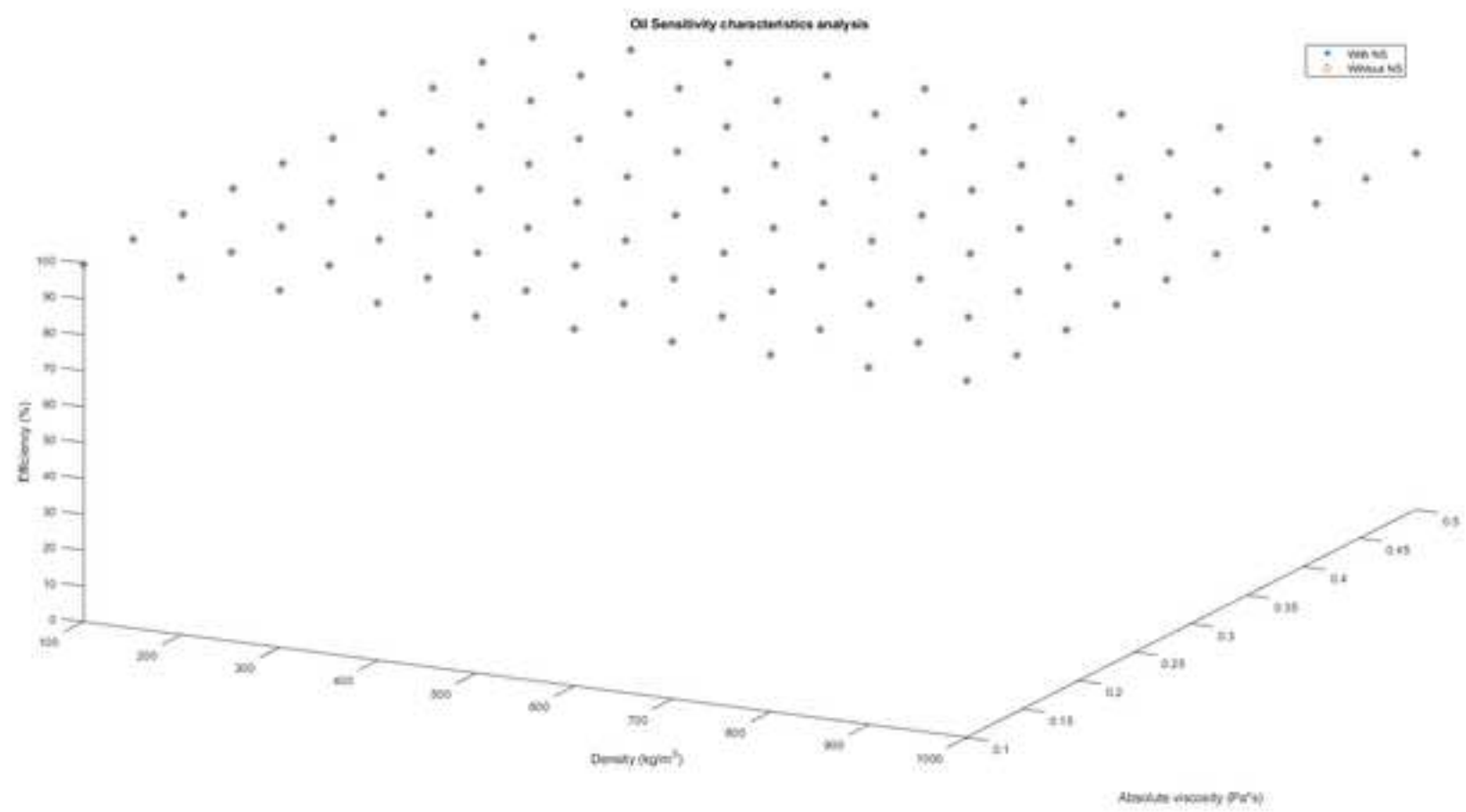
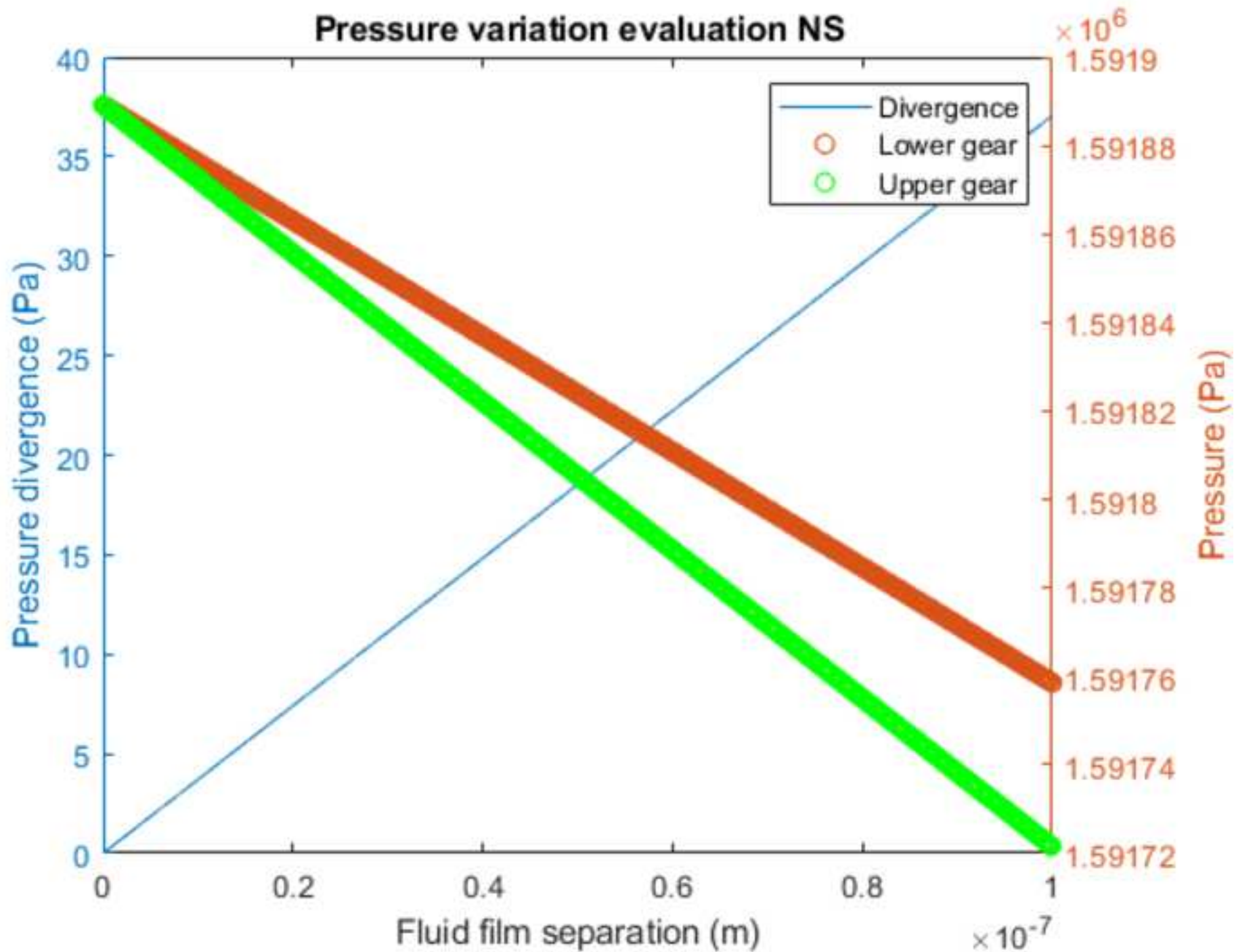
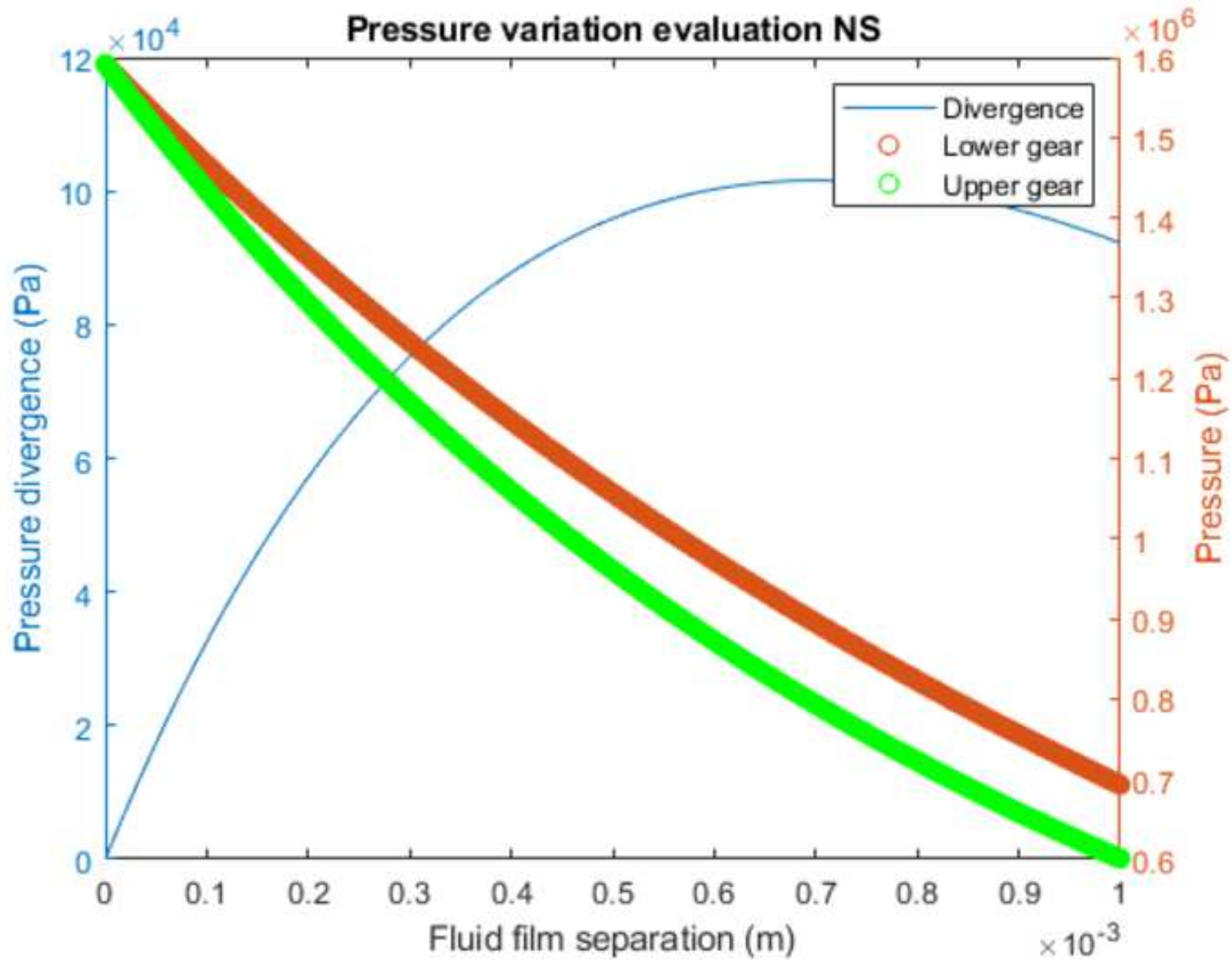


Figure 7

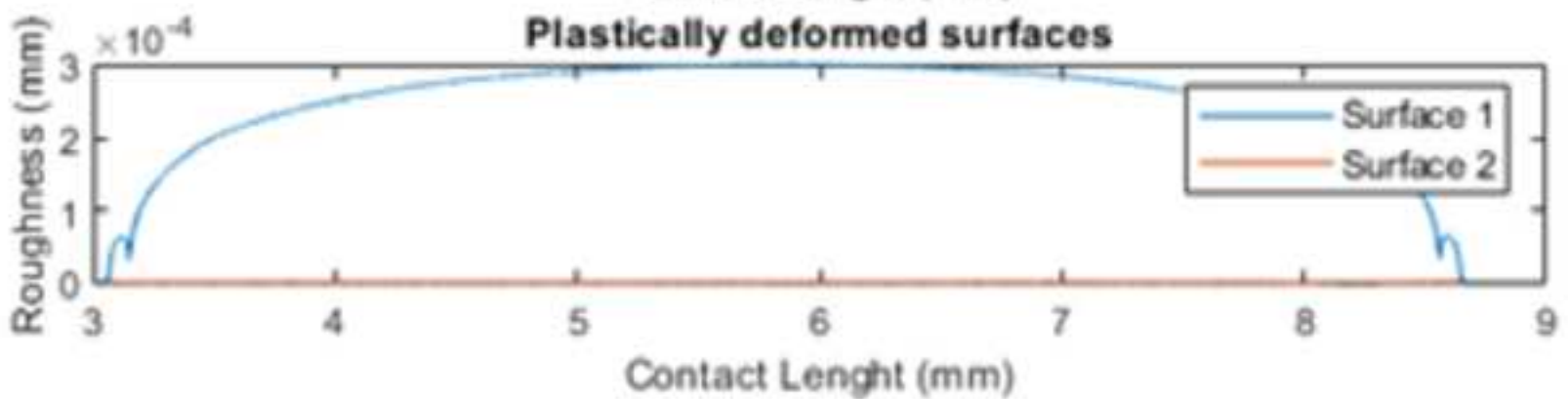
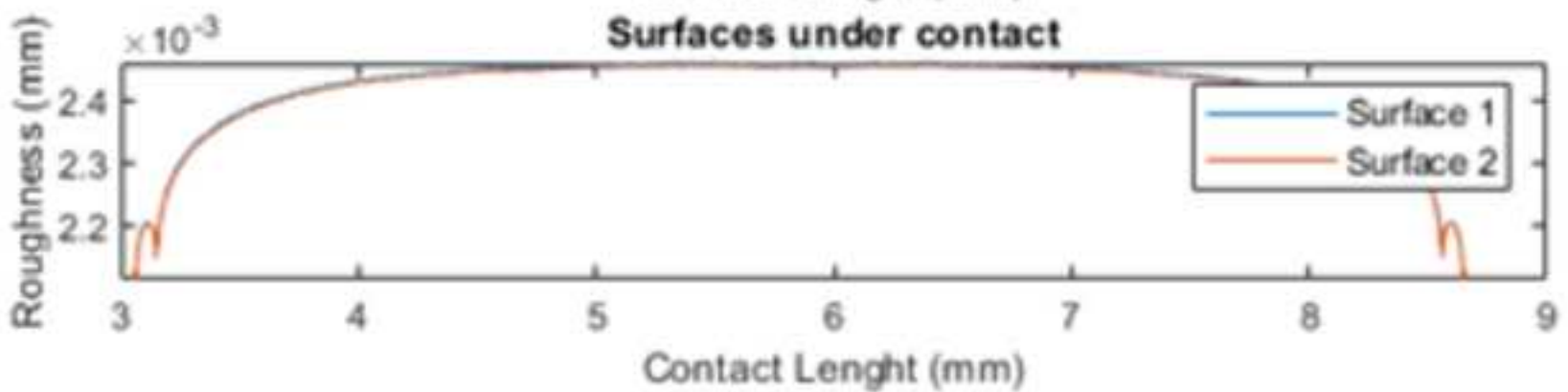
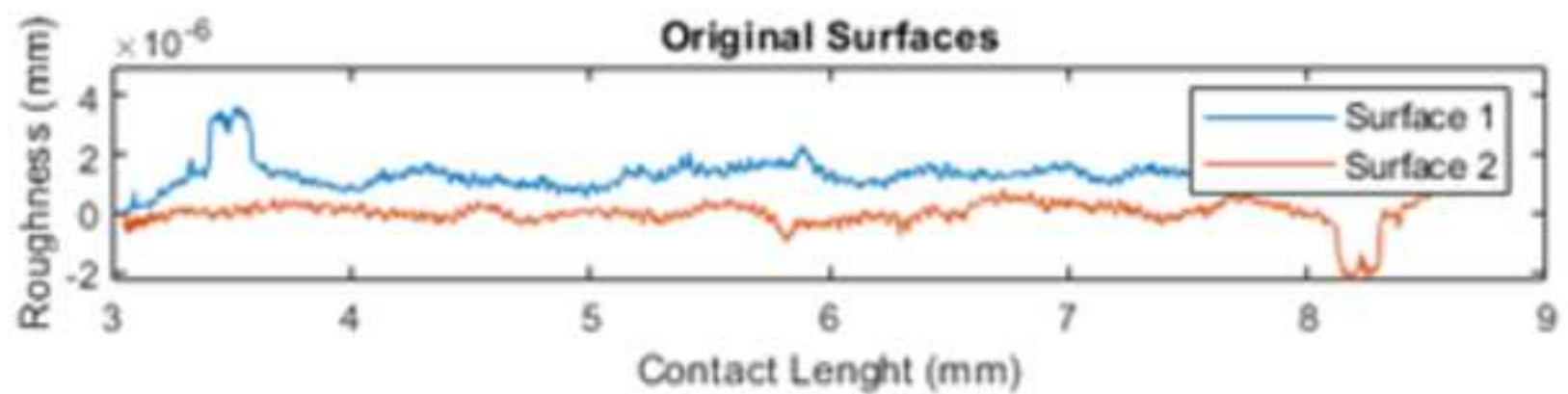
[Click here to access/download;Figure;Figure 7 Lubricant sensitivity and NS validation analysis.png](#)



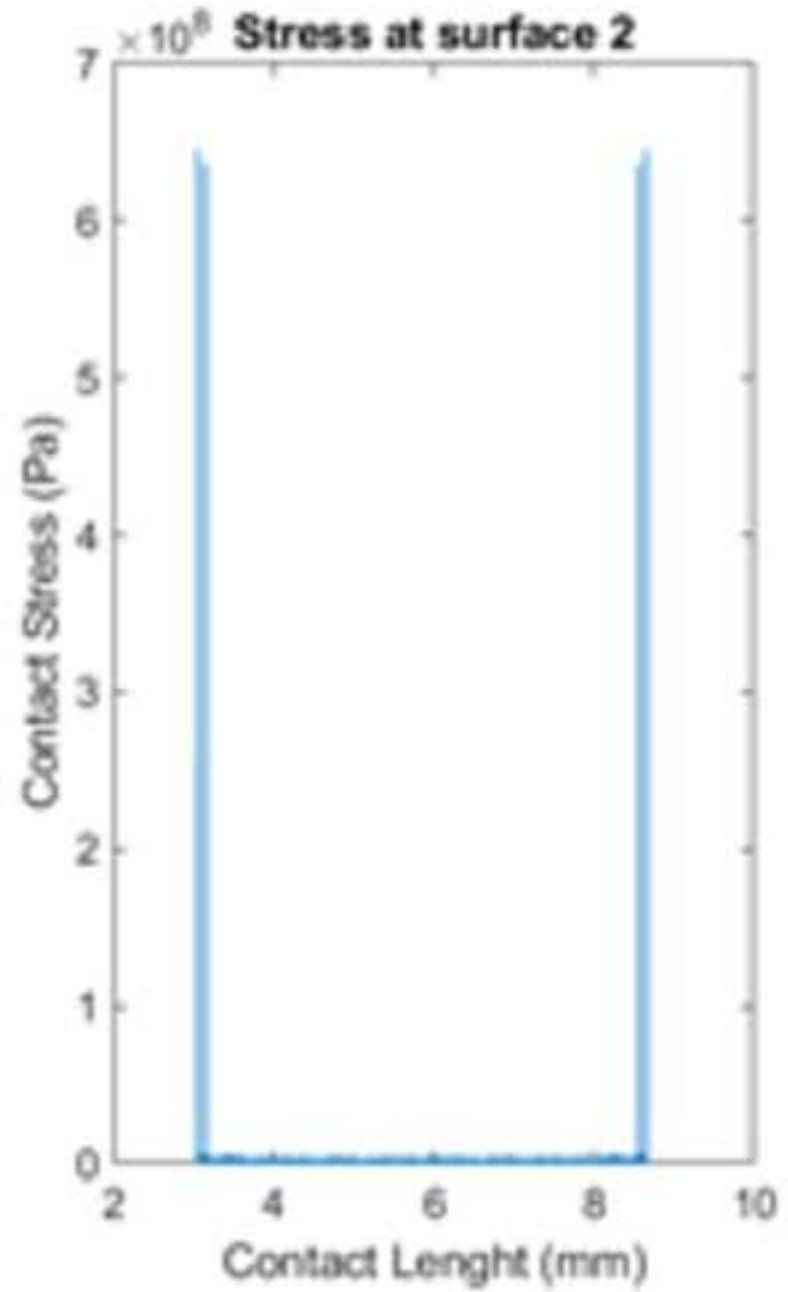
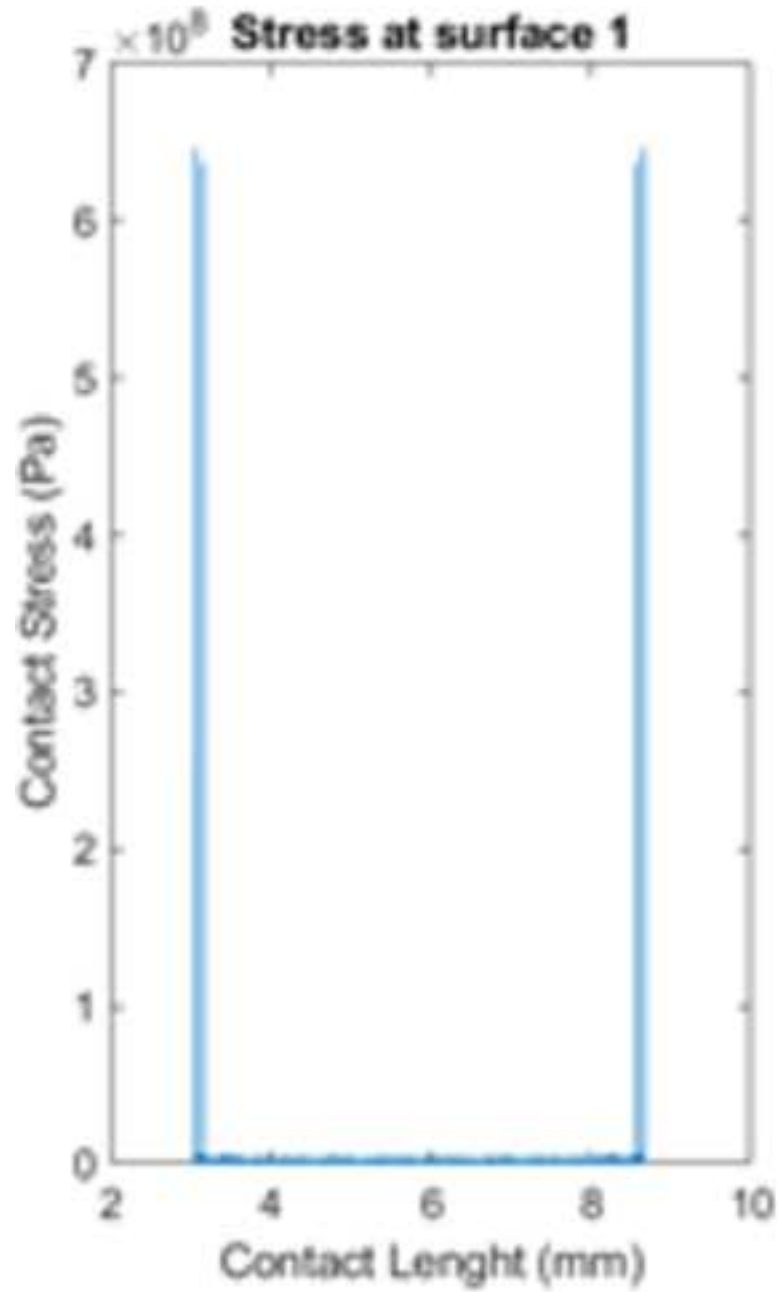




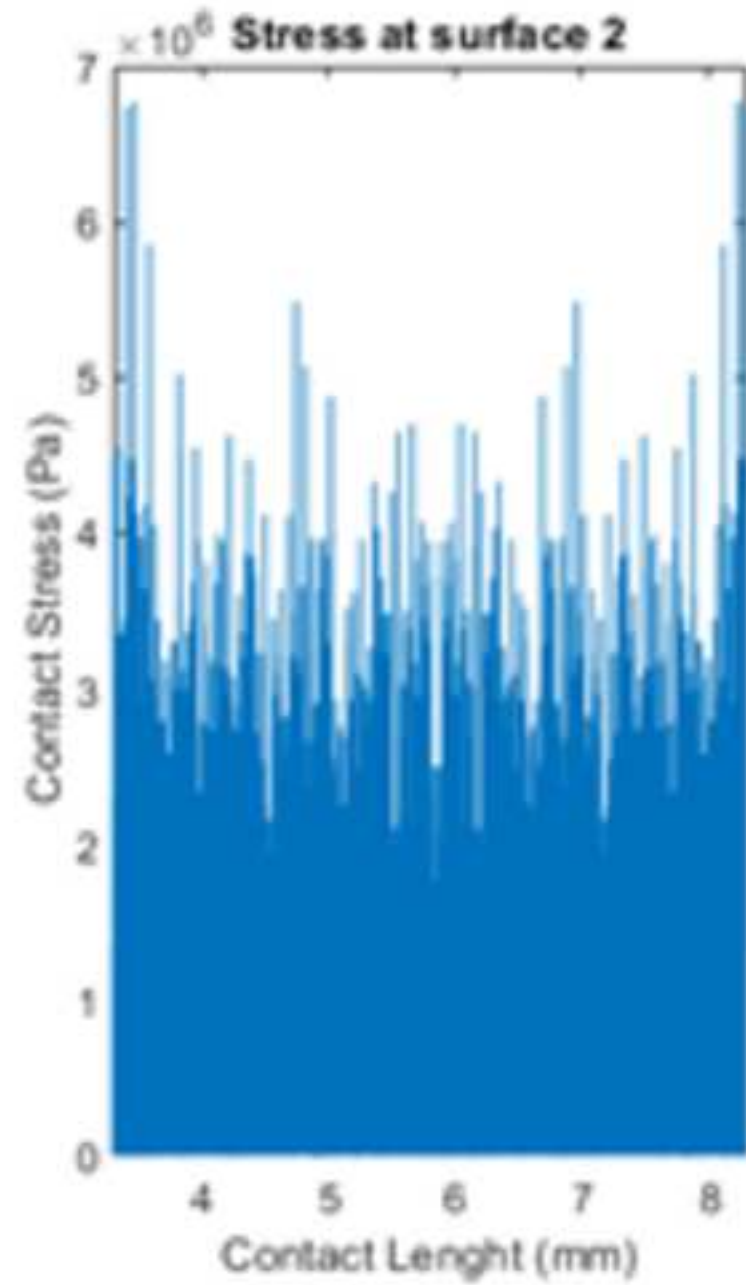
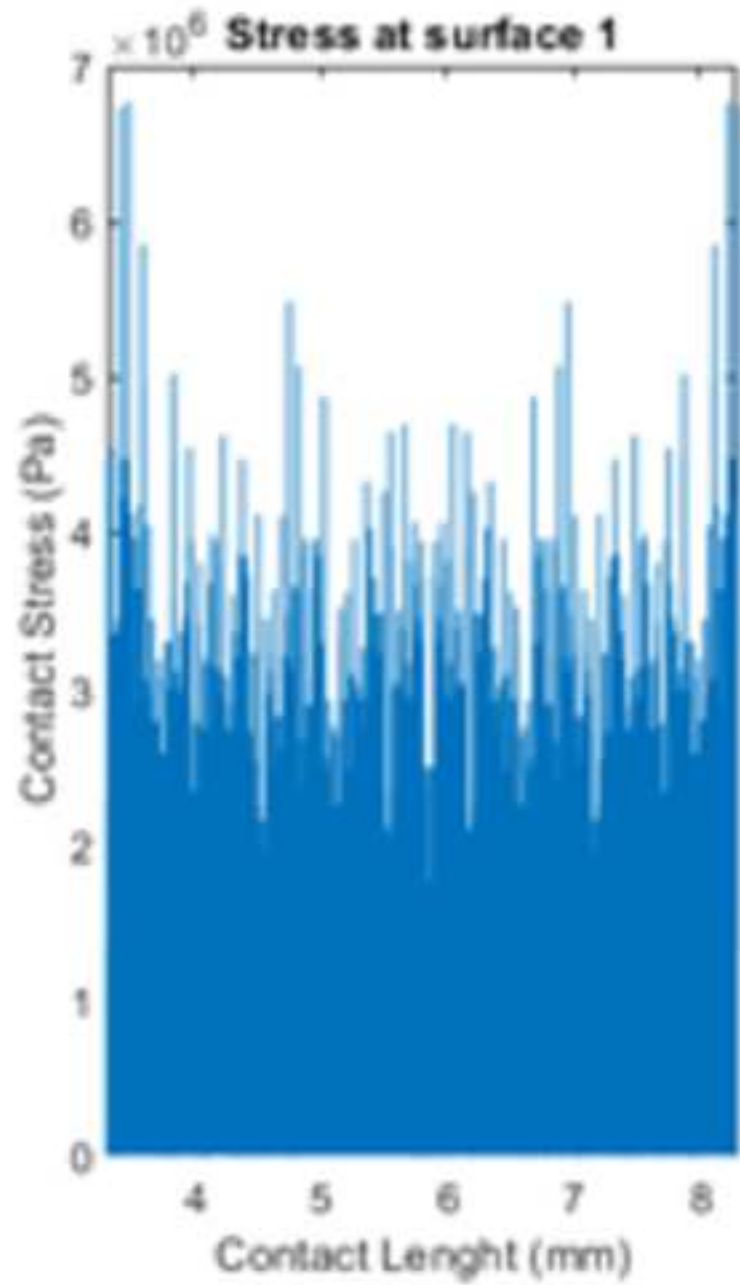
Surface variation over contact



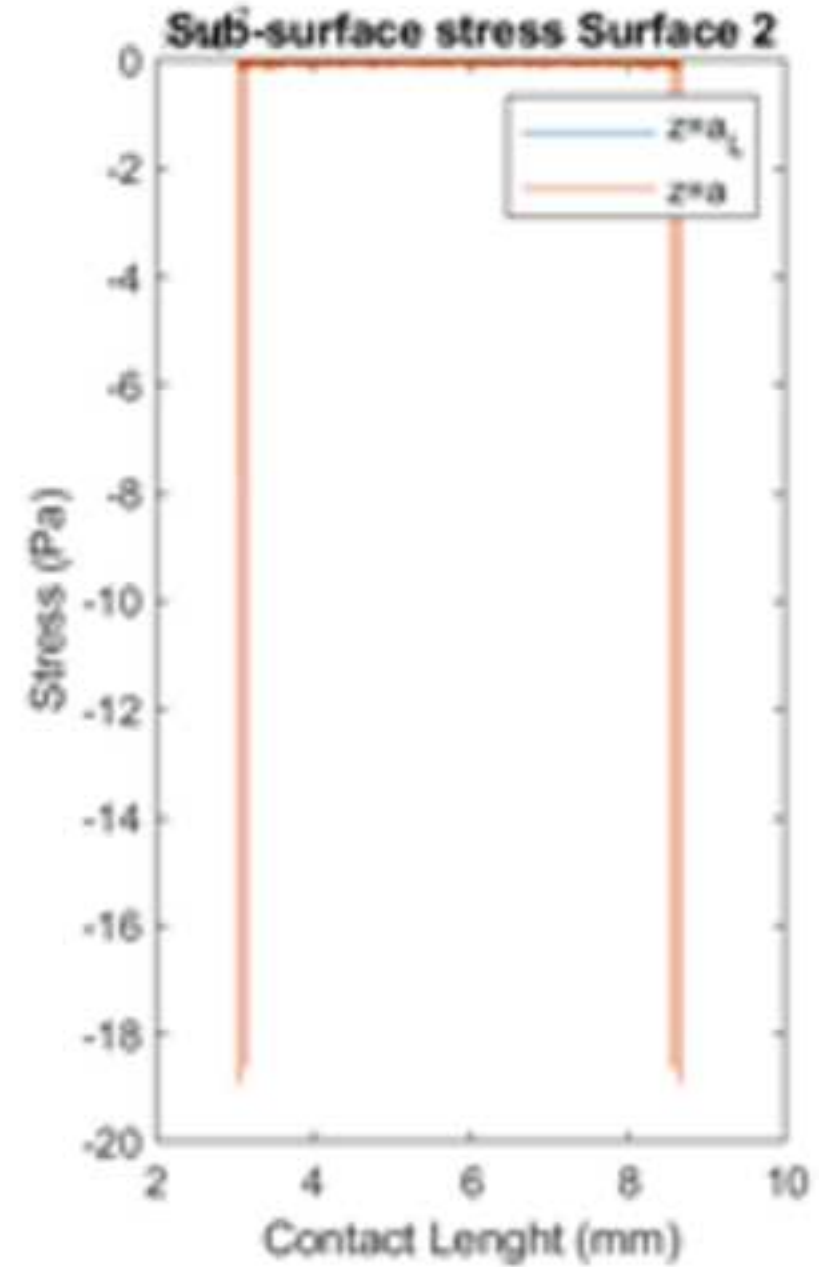
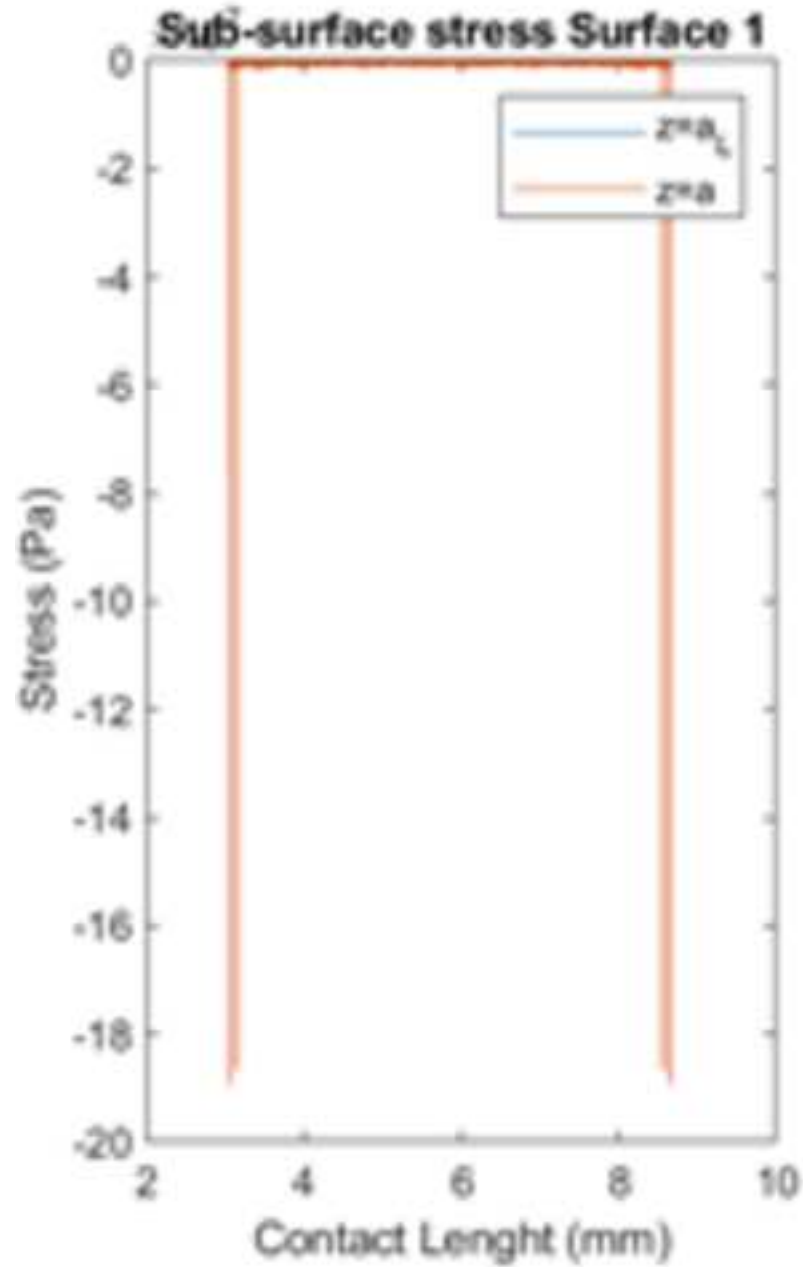
Surface Contact Stress



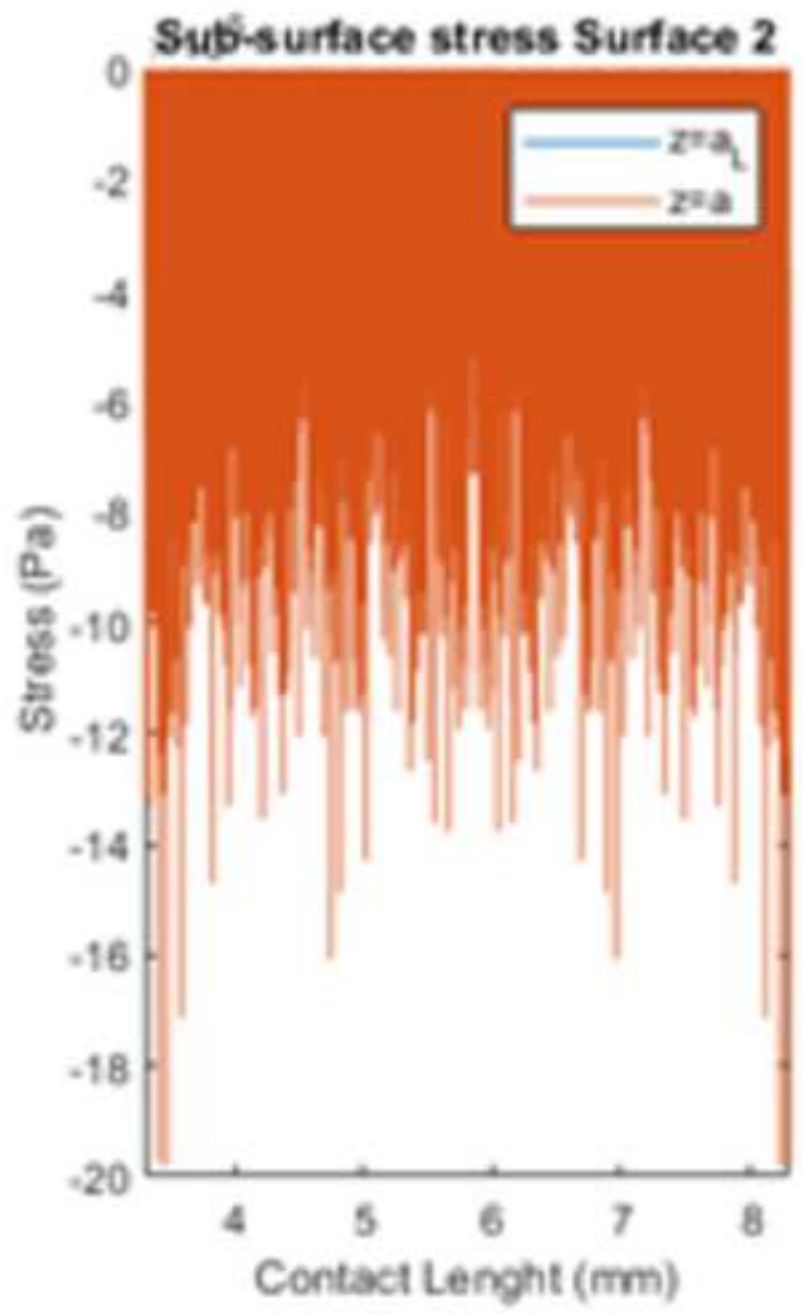
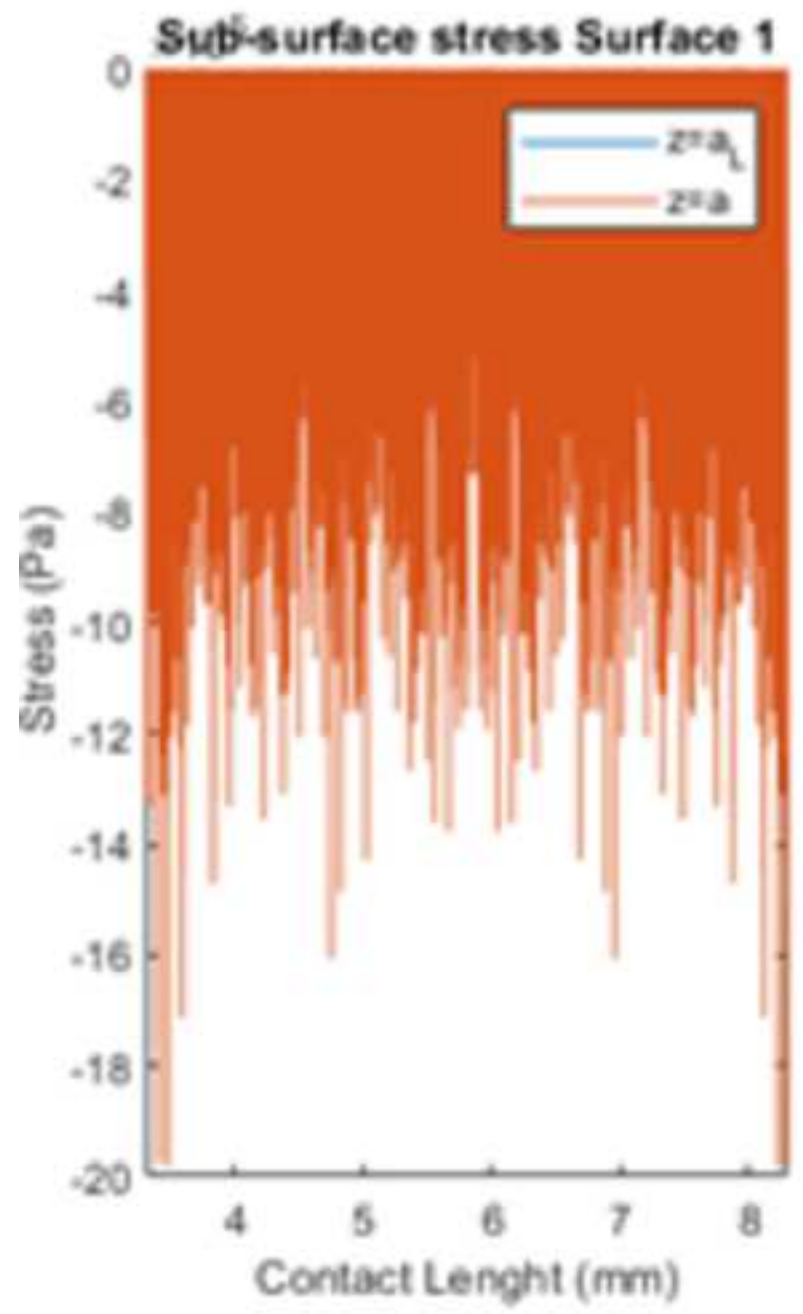
Surface Contact Stress



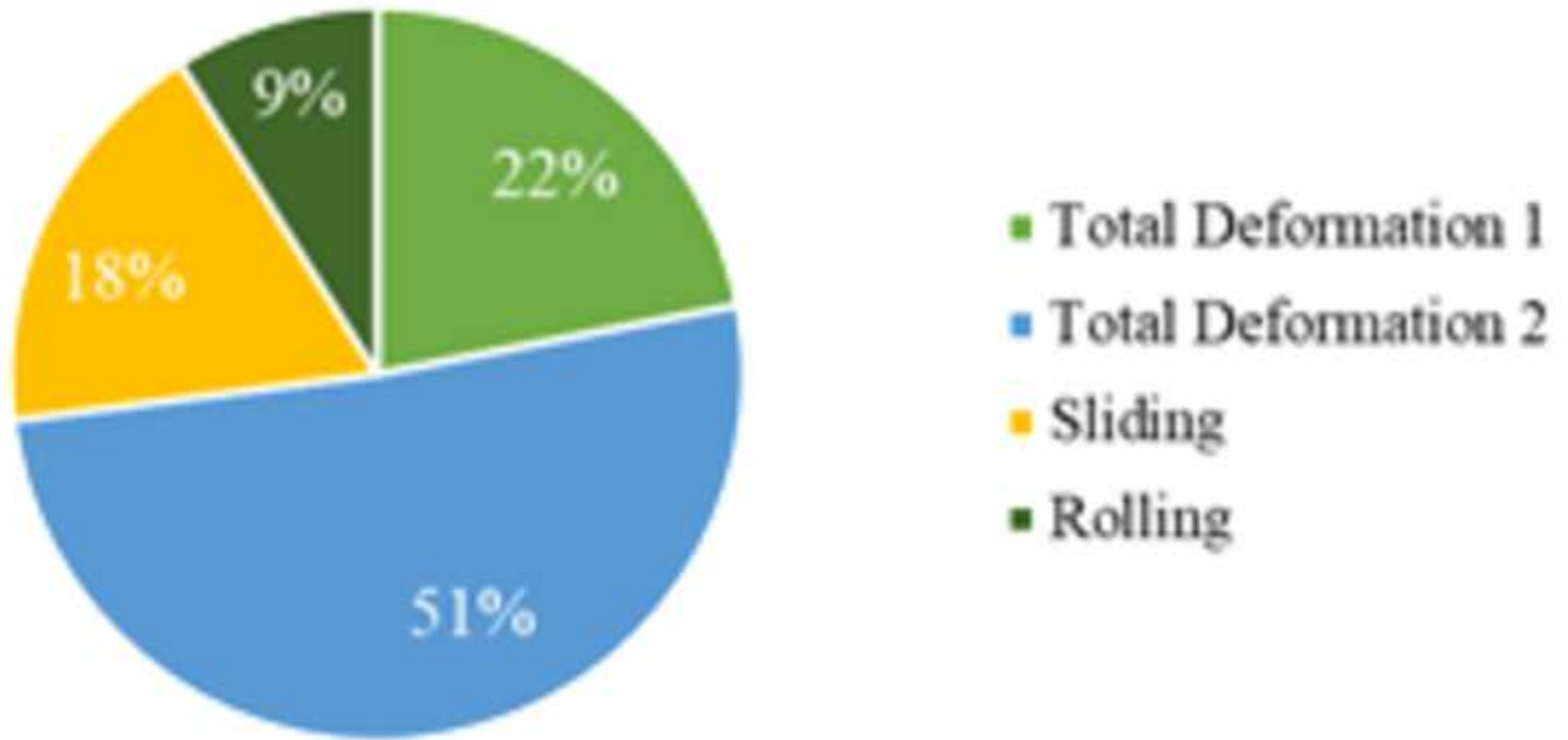
Sub-Surface Stress distribution



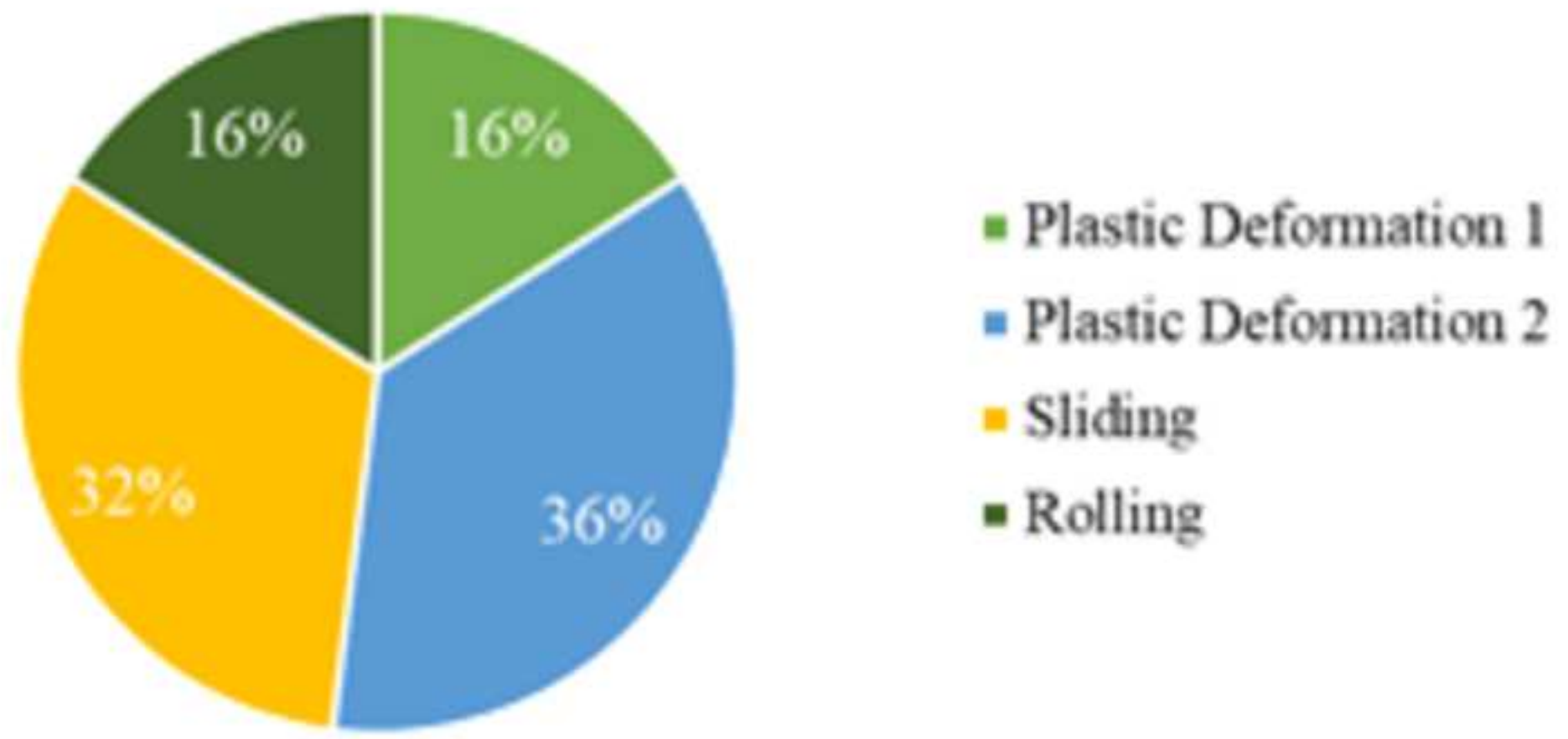
Sub-Surface Stress distribution

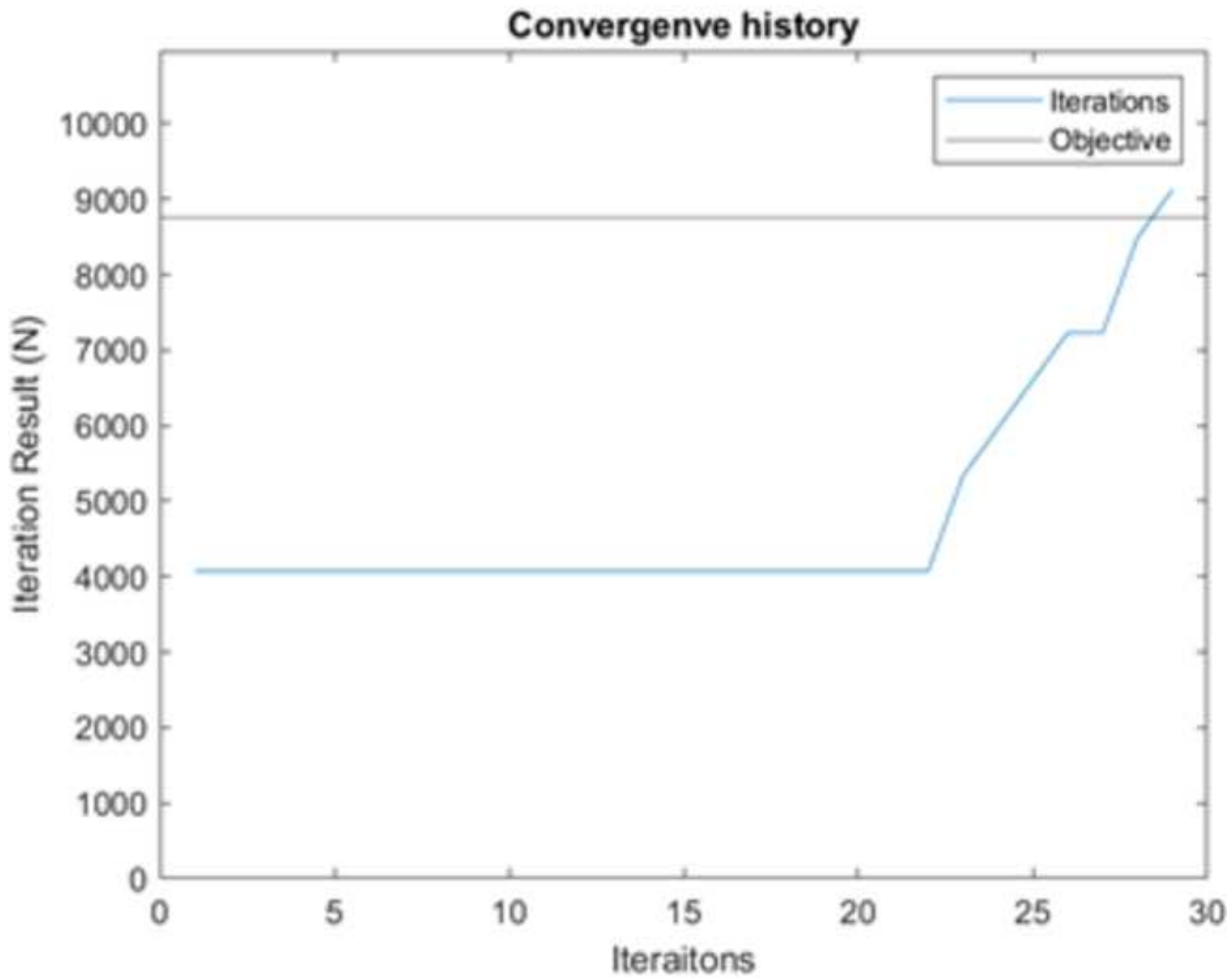


Energy loss distribution in contact



Energy loss distribution after contact





1. References

- [1] M. Sosa, "Running-in of gears- surface and efficiency transformacion," KTH, Stockholm, 2017.
- [2] S. B. a. B. R. L. Xiao, "The influence of surface roughness and the contact pressure distribution on friction rolling/sliding contacts," *Tribology international*, pp. 40:4:694-698, 2007.
- [3] S. Björklund, "Elastic contacts between rough surfaces.," KTH, Stockholm, 1995.
- [4] K. Johnson, "Contact Mechanics," Cambridge University Press, Cambridge, 1987.
- [5] H. e. al, "Prediction of Mechanical Efficiency of Parallel-Axis Gear Pairs," *Journal of Mechanical Engineering* 129, pp. 58-68, 2007.
- [6] P. R. a. A. Kadiric, "The influence of side-roll ratio on the extent of micropitting damage in rolling-sliding contacts pertinent to gear applications," *Tribology Letters*, pp. 67:1-20, 2019.
- [7] Y. M. a. V. Myunster, "Determination of power losses in gear transmissions with rolling and slidding friction incorporated," *Mechanisms and Machine Theory*, pp. 37: 167-174, 2002.
- [8] P. M. e. al, "Gear Solutions," 15 04 2021. [Online]. Available: <https://gearsolutions.com/features/predicting-gear-sliding-losses/>.
- [9] S. W. e. al, "A Frictional Model of Partial-EHL Contacts and its Applications to Power Loss in Spur Gears," *Tribology Transactions* 34, pp. 398-407, 1991.
- [10] "Chapter 2: Overall Methodology," in *DEVELOPMENT OF A GENERALIZED MECHANICAL EFFICIENCY PREDICTION METHODOLOGY FOR GEAR PAIRS*, Columbus, Ohio State University, 2005, p. 30.
- [11] m. M. e. M.M.Khonsari, "The high pressure rheology of some simple model hydrocarbons," *Tribology International* 82, pp. 228-244, 2015.
- [12] M. B. e. R. L. Jonny Hansen, "A New Film Parameter for Rough Surface EHL Contacts with Anisotropic and Isotropic Structures," *Tribology Letters* 69:37, pp. 1-17, 2021.
- [13] J. Hansen, "Elasto-hydrodynamic film formation in heavily loaded rolling-sliding contacts," Lulea University of Technology, Gothenburg, 2021.
- [14] I.-T. a. M. M. Hui Long, "Analytical and Experimental Study of Gear Surface Micropitting due to Variable Loading," *Applied Mechanics and Materials*, pp. 750: 96-103, 2015.
- [15] M. Tomic, "Model of Thermal EHL Based on Navier-Stokes Equations: Effects of asperities and Extreme Loads," *Lulea University of Technology*, pp. 1-82, 2019.
- [16] D. S. Dizdar, "High-Performance Sintered-Steel Gears for Transmissions and Machinery: A Critical Review," *GEARTECHNOLOGY*, pp. 60-65, 2012.
- [17] X. Li, "Efficiency and wear properties of spur gears made of powder metallurgy materials," KTH Royal Institute of Technology, Stockholm, 2016.

- [18] D. G. Kotthoff, "NVH Potential of PM Gears for Electrified Drivetrains," *GEARTECHNOLOGY*, pp. 40-43, 2018.
- [19] E. Bergseth, "On tribological design in gear tooth contacts," Royal Institute of Technology, Stockholm, 2012.
- [20] H. U. Jamali, K. Sharif and H. E. a. R. Snide, "Transient EHL analysis of helical gears," in *International Gear Conference 2014*, Lyon, 2014.
- [21] R. M. Abraham, "AN EXPERIMENTAL STUDY OF SCUFFING PERFORMANCE OF A HELICAL GEAR PAIR SUBJECTED TO DIFFERENT LUBRICATION METHODS," Ohio State University, Columbus, 2014.
- [22] W. B. Rowe, "18 - Energy Partition and Temperatures," in *Principle of Modern Grinding Technology*, Norwich, William Andrew Publishing, 2014, pp. 381-420.
- [23] C-Therm, "C-Therm," 25 04 2022. [Online]. Available: <https://ctherm.com/resources/helpful-links-tools/thermalresistanceandconductivity/>.
- [24] T. Ishizaki and T. I. a. H. Nagano, "Measurement of local thermal contact resistance with a periodic heating method using microscale lock-in thermography," *Review of Scientific Instruments*, p. 91: 064901, 2020.
- [25] C. Zhou, M. Xing and H. W. a. B. Hu, "A novel thermal network model for predicting the contact temperature of contact gears," *International Journal of Thermal Sciences*, p. 161:106703, 2021.

Table 1 Adimensional EHL coefficients

Surface roughness direction	α (-)	γ_1 (-)	γ_2 (-)	γ_3 (-)
Isotropic & transversal	1.134 - X	0.61	0.75	$2/\pi$
Longitudinal	1.146 - X	1	1.23	$2/3$

Table 1 Input variables for validation run

Variable	Value	Units	Variable	Value	Units
Module	1.3	mm	Elastic limit 2	235	MPa
Pressure angle	20	deg	Bulk temperature 1	60	K
Helix angle	30	deg	Bulk temperature 2	60	K
Number teeth 1	50	-	Lubricant conductivity	0.135	W/m/K
Number teeth 2	120	-	Lubricant heat capacity	2	J/g/K
Width 1	50	mm	Thermal conductivity 1	45	W/m/K
Width 2	50	mm	Thermal conductivity 2	45	W/m/K
Input moment	285	Nm	Lubricant density	998	Kg/m ³
Input rotational speed	3000	rpm	Lubricant load loss dependent coefficient	0.84	-
Metal-to-metal friction coefficient	0.3	-	Reference load loss dependent coefficient	0.9069	-
Young's modulus 1	210	GPa	Lubricant absolute pressure	0.0975	Pa·s
Young's modulus 2	210	GPa	Lubricant's pressure viscosity coefficient	2e-08	mm ² /N
Poisson Coefficient 1	0.3	-	Numerical error	1	%
Poisson Coefficient 2	0.3	-	Delta step	80	nm
Elastic limit 1	235	MPa			